




Research Article

Adaptive Fuzzy Modified Fixed-Time Fault-Tolerant Control on SE(3) for Coupled Spacecraft

Yafei Mei ¹, Ying Liao ¹, Kejie Gong ¹ and Da Luo²

¹College of Aerospace Science and Engineering, National University of Defense Technology, No. 109 Deya Road, Changsha 410073, Hunan, China

²Shanghai Institute of Satellite Engineering, Shanghai 201109, China

Correspondence should be addressed to Yafei Mei; meiyafei@nudt.edu.cn

Received 2 November 2020; Revised 18 December 2020; Accepted 28 December 2020; Published 11 January 2021

Academic Editor: Yong Chen

Copyright © 2021 Yafei Mei et al. This is an open access article distributed under the Creative Commons Attribution License, which permits unrestricted use, distribution, and reproduction in any medium, provided the original work is properly cited.

This paper aims to solve the control problem of coupled spacecraft tracking maneuver in the case of actuator faults, inertia parametric uncertainties, and external disturbances. Firstly, the spacecraft attitude and position coupling kinematics and dynamics model are established on the Lie group SE(3), and the coupled relative motion tracking error model is derived by exponential coordinates. Then, considering the actuator faults, an adaptive fuzzy scheme is proposed to estimate the lumped disturbances in real time, and a novel modified fixed-time terminal sliding mode fault-tolerant control law is developed to deal with the actuator faults and compensate the lumped disturbances. Next, the Lyapunov method is used to prove the stability and convergence of the system. Finally, the proposed controller can achieve fast and high-precision fault-tolerant control goals, and its effectiveness and feasibility are verified by numerical simulation.

1. Introduction

In the context of the rapid development of space technology, new and higher requirements have been put forward for the mobility and accuracy of spacecraft. The modeling and control of the attitude and trajectory of relatively moving spacecraft has always been a hot research topic in the fields of space rendezvous and docking, spacecraft formation flying (SFF) [1, 2]. Due to the strong coupling and nonlinearity of the relative motion of spacecraft's attitude and position motion, the conventional idea of dividing attitude and position motion into independent two-channel control ignores the influence of coupling between the two, although it satisfies the requirements of some space missions. However, for aerospace missions with high-precision requirements, the divide-and-conquer method will appear powerless [3]. Therefore, seeking the integrated control of spacecraft attitude and position has theoretical guidance and is of great significance to engineering practice.

Due to long-term exposure to harsh space environments such as strong radiation and ultra-low temperature, the actuator will have various types of failures. Therefore, the

conventional control theory based on the normal operation of the actuator may be difficult to cope with the failure and may eventually cause the system to crash or fail. In addition, the spacecraft itself will also face the uncertainty of internal parameters and external disturbances, which brings huge challenges to the design of the control system. So it is particularly important to choose a suitable fault-tolerant control strategy for the aforementioned drawbacks, which also provides a strong guarantee for the long-term service operation of the spacecraft.

At present, many research results have been made on the problem of spacecraft attitude fault-tolerant control [4, 5]. But for the spacecraft attitude and position coupling control system, when various faults occur in the relative attitude and position actuators at the same time, the related six-degree-of-freedom (6-DOF) fault-tolerant control algorithm design is not enough [6]. Dong et al. [7, 8], studied the integrated fault-tolerant control of the spacecraft's position and attitude in the case of actuator failure based on the dual quaternion, and their numerical simulation results verified the effectiveness of the algorithm.

In recent years, the coupled modeling of rotation and translation relative motion based on different forms of rigid spacecraft has attracted widespread attention. Common spacecraft attitude and position coupling modeling and control forms mainly include dual quaternion [7, 8], Lie group $SE(3)$ [9, 10], modified Rodrigues parameters (MRPs), and other forms [11, 12]. Although the integrated modeling method of spacecraft attitude and position based on dual quaternion is widely used, dual quaternion also has its limitations. The model based on dual quaternion uses eight parameters to describe the three-dimensional motion, so it requires unitized constraints. Sometimes improper handling of this constraint will cause problems. Moreover, since the group function corresponding to the unit quaternion is left multiplication and right multiplication, the quaternion description rotation is not unique, which will cause ambiguity, and when it is serious, it will cause unwinding problem [3]. Moreover, describing the attitude based on MRPs is nonglobal and nonunique [13]. Compared with the traditional description method in Euclidean space, the geometric framework of Lie group $SE(3)$ is more natural and concise, the analysis results are more realistic and credible, and the designed controller is more concise, so in recent years, it received attention gradually. Lie group $SE(3)$ can describe the three-dimensional translation and rotation of a rigid body. Lee et al. [14], Sanyal et al. [15], and Bullo and Murray [16], conducted an in-depth study on the control of the 6-DOF motion of a spacecraft on $SE(3)$. By using the relationship between the exponential mapping function and the logarithm mapping function of Lie group and Lie algebra, the motion spinor is transformed into the corresponding spacecraft attitude and position motion equation. On this basis, various simple controllers are designed to realize the pose tracking control target [17]. In this paper, the integrated model of spacecraft attitude and position coupling is established in the framework of Lie group $SE(3)$, which is convenient for the design of fault-tolerant controllers in the following.

Fault-tolerant control mainly includes active fault-tolerant control and passive fault-tolerant control. Among them, considering the actuator failure belongs to the integrity design category of passive fault-tolerant control, it is also a hot research direction in the field of fault-tolerant control and has obtained rich research results [18–22]. Fuzzy approximation can make full use of the information ability of fuzzy logic systems; it is easier to construct and can approximate nonlinear functions with arbitrary accuracy. When the actuator fails, the uncertainty of the system increases. For the parameter uncertain system, the adaptive law can be constructed by the Lyapunov method, and the uncertain parameters in the model can be replaced by the adaptive control based on the principle of equivalence. Finally, the adaptive law is designed for the estimated parameters to make the closed-loop system stable. This mainstream adaptive control method has been widely used in the field of spacecraft control due to its simple design and easy to understand [23]. Recently, many major achievements in the engineering application of fuzzy approximation methods have been reported, such as application of adaptive fuzzy controller in industrial process [24, 25]. At

the same time, fuzzy control is also applied to robust fault-tolerant control for fault detection and actuator faults [26–29]. In addition, the fuzzy control scheme to approximate the disturbance of the spacecraft has been successfully applied, and it is effective to combine the adaptive fuzzy controller of NFTSMC in [30, 31] to reject the system uncertainty. Zhang et al. [32] applied fuzzy adaptive finite-time control to the 6-DOF SFF system and achieved success when considering the consensus control problem among the followers with signal transmission time delays.

Fixed-time control is developed on the basis of finite-time control. The difference between the two is only in the form of the sliding surface. The former can achieve fixed-time convergence without relying on the initial state, while the latter's convergence time is related to the initial state. Double-power fast terminal sliding mode control is a kind of fixed time control, which can be used to realize the fixed time stability of the system, which is more useful than the finite-time sliding mode control methods, such as terminal sliding mode (TSM) [33], fast terminal sliding mode (FTSM) [34], and nonsingular fast terminal sliding mode (NFTSM) [35]. It has faster convergence speed and better control effect. Shi et al. achieved attitude tracking control of rigid spacecraft on Lie group with fixed-time convergence [36] and global fixed time attitude tracking control for the rigid spacecraft with actuator saturation and faults [37]. Gao et al. proposed adaptive fixed time attitude tracking control for rigid spacecraft with actuator faults on MRPs [38]. Gong et al. proposed modified adaptive fixed-time terminal sliding mode control on $SE(3)$ for coupled spacecraft tracking maneuver [3]. Mobayen et al. [39] proposed a new adaptive finite-time stabilization method based on global sliding mode to advance the steady state and transient performances of a class of chaotic flows in the presence of disturbances. Also, Mobayen and Pujol-Vázquez used robust LMI approach to deal with nonlinear feedback stabilization of continuous state-delay systems with lipschitzian nonlinearities and verified the effectiveness through experiments [40]. Jafari and Mobayen [41] combined LMI approach and second-order sliding set design for a class of uncertain nonlinear systems with disturbances.

Motivated by the facts mentioned above, this paper takes the leader-follower formation spacecraft as the research object. Firstly, a dynamic model of the relative tracking error of the spacecraft attitude and position coupling with model uncertainties, external disturbances, and actuator faults is derived on the Lie group $SE(3)$. Then, the adaptive fuzzy method is used to design the sliding mode controller to realize the fixed-time fault-tolerant control.

The novelty of this paper is as follows: inspired by [3, 32], the proposed model in this paper takes the actuator faults into consideration. Based on the established model, a modified double-power fast terminal sliding manifold is defined by the exponential coordinates and velocity tracking errors, and then adaptive fuzzy modified fixed-time fault-tolerant control schemes is proposed, in which the adaptive fuzzy control technique is applied to reject the system lumped disturbances. Compared with finite-time stability and traditional fixed time stability, the control performance

obtained in this paper has significant advantages in convergence accuracy and effectiveness.

The structure of this paper is as follows: Section 2 introduces the mathematics preliminaries and the rigid body dynamics of the spacecraft on $SE(3)$ with actuator faults. Section 3 adopts fuzzy adaptive method to design the sliding mode controller to realize the modified fixed-time fault-tolerant control and uses the Lyapunov method to prove the stability of the system strictly. Section 4 verifies the effectiveness of this method through numerical simulation. Section 5 draws conclusions and summarizes this paper.

2. Mathematics Preliminaries

In order to facilitate the design and stability proof and analysis of the integrated attitude and position control system, the following will give some related definitions and stability theory and lemmas.

2.1. Notations. For any column vector $\mathbf{x} = [x_1, x_2, \dots, x_n]^T \in \mathbb{R}^n$, define the following vector and operation:

- (1) $|\mathbf{x}|^\alpha = [|x_1|^\alpha, |x_2|^\alpha, \dots, |x_n|^\alpha]^T$, where $|\cdot|$ is the absolute value.
- (2) $\|\mathbf{x}\|$ denotes the Euclidean norm or its induced norm.
- (3) $\text{sig}^\alpha(\mathbf{x}) = |\mathbf{x}|^\alpha \text{sgn}(\mathbf{x}) = [|x_1|^\alpha \text{sgn}(x_1), |x_2|^\alpha \text{sgn}(x_2), \dots, |x_n|^\alpha \text{sgn}(x_n)]^T$, where $\text{sgn}(\cdot)$ is the sign function.
- (4) $(d|\mathbf{x}|^\alpha/dt) = \text{diag}[\alpha \text{sig}^{\alpha-1}(\mathbf{x})] \dot{\mathbf{x}}$,
 $(d\text{sig}^\alpha(\mathbf{x})/dt) = \text{diag}[\alpha |\mathbf{x}|^{\alpha-1}] \dot{\mathbf{x}}$.

- (5) $[\cdot]^\wedge$ represents an operator that maps a vector to a Lie algebra. For $\mathfrak{ce}(3)$, it maps a vector to an skew-symmetric matrix, that is, $\mathbf{u}^\wedge = \begin{bmatrix} 0 & -u_z & u_y \\ u_z & 0 & -u_x \\ -u_y & u_x & 0 \end{bmatrix}$;

$[\cdot]^\vee$ represents the operator that maps the Lie algebra to a vector. For $\mathfrak{ce}(3)$, it maps the skew-symmetric

matrix to a vector, which is $\begin{bmatrix} 0 & -u_z & u_y \\ u_z & 0 & -u_x \\ -u_y & u_x & 0 \end{bmatrix}^\vee = \mathbf{u}$.

2.2. Relative Coupled Dynamics of Spacecraft on Lie Group $SE(3)$. Firstly, in order to describe the space orientation of the leader-follower spacecraft and establish the kinematics and dynamics model, we introduce three reference frames that are all orthogonal coordinate systems as shown in Figure 1. The Earth-centered inertial (ECI) reference frame with the origin at the center of the Earth is represented by $\{I\} = \{x_I, y_I, z_I\}$, which is used to describe the absolute motion of the spacecraft relative to the Earth. The body-fixed frames of the leader spacecraft and the follower spacecraft can be expressed as $\{Lb\} = \{x_{Lb}, y_{Lb}, z_{Lb}\}$ and $\{Fb\} = \{x_{Fb}, y_{Fb}, z_{Fb}\}$, respectively; their origin is at the center of mass of the spacecraft, and the axis coincides with the principal axis of inertia.

In nature, the configuration space of rigid body motion is $SE(3)$, which can express translation and rotation of rigid

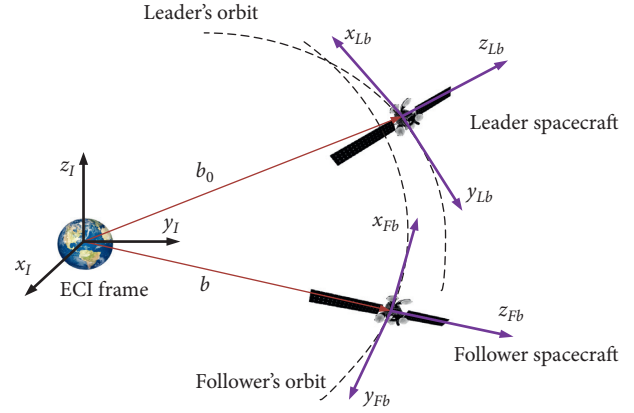


FIGURE 1: The relative motion and coordinate reference frames definition of the leader-follower spacecraft.

body compactly. The special Euclidean group $SE(3)$ is the semidirect product of the three-dimensional Euclidean space and the special orthogonal space, which can be expressed as $SE(3) = \mathbb{R}^3 \ltimes SO(3)$. \mathbb{R}^3 is used to describe the translation of the rigid body's center of mass; $SO(3) = \{\mathbf{R} \in \mathbb{R}^{3 \times 3} | \mathbf{R}\mathbf{R}^T = \mathbf{I}, \det(\mathbf{R}) = 1\}$ is a rotation group composed of a three-dimensional rotation matrix, which is used to represent the rotation of the rigid body around the center of mass. Therefore, an element \mathbf{g} in the Lie group $SE(3)$ can express the configuration of the spacecraft [3]:

$$\mathbf{g} = \begin{bmatrix} \mathbf{R} & \mathbf{b} \\ \mathbf{0}_{1 \times 3} & 1 \end{bmatrix} \in SE(3), \quad (1)$$

where $\mathbf{R} \in SO(3)$ is the rotation matrix of the spacecraft from the body-fixed frame to the ECI reference frame and $\mathbf{b} \in \mathbb{R}^3$ is the position vector from the center of mass of the Earth to the center of mass of the spacecraft in the ECI coordinate system.

The angular velocity and translational velocity of the spacecraft are defined as

$$\xi = \begin{bmatrix} \mathbf{v} \\ \boldsymbol{\omega} \end{bmatrix} \in \mathbb{R}^6. \quad (2)$$

The above velocity vectors are defined in the body-fixed frame of the spacecraft. To describe the kinematics and dynamics equations below, it is necessary to introduce the Lie group $SE(3)$ and its corresponding Lie algebra $\mathfrak{ce}(3)$ to meet the following mapping relations:

$$\xi = \begin{bmatrix} \mathbf{v} \\ \boldsymbol{\omega} \end{bmatrix} \in \mathbb{R}^6. \quad (3)$$

The adjoint matrix of $\mathbf{g} = \mathbf{g}(\mathbf{R}, \mathbf{b}) \in SE(3)$ can be expressed as

$$\text{Ad}_{\mathbf{g}} = \begin{bmatrix} \mathbf{R} & \mathbf{b}^\wedge \mathbf{R} \\ \mathbf{0}_{3 \times 3} & \mathbf{R} \end{bmatrix} \in \mathbb{R}^{6 \times 6}. \quad (4)$$

The Lie algebra corresponding to $\xi = [\mathbf{v}^T \ \boldsymbol{\omega}^T]^T$ can be expressed as

$$\xi^\wedge = \begin{bmatrix} \boldsymbol{\omega}^\wedge & \mathbf{v} \\ 0_{1 \times 3} & 0 \end{bmatrix} \in \mathfrak{ce}(3). \quad (5)$$

The adjoint matrix of $\xi^\wedge = \xi^\wedge(\boldsymbol{\omega}, \mathbf{v}) \in \mathfrak{ce}(3)$ can be expressed as

$$\text{ad}_\xi = \begin{bmatrix} \boldsymbol{\omega}^\wedge & \mathbf{v}^\wedge \\ 0_{3 \times 3} & \boldsymbol{\omega}^\wedge \end{bmatrix} \in \mathbb{R}^{6 \times 6}. \quad (6)$$

The co-adjoint matrix of $\xi^\wedge = \xi^\wedge(\boldsymbol{\omega}, \mathbf{v}) \in \mathfrak{ce}(3)$ can be expressed as

$$\text{ad}_\xi^* = (\text{ad}_\xi)^T = \begin{bmatrix} -\boldsymbol{\omega}^\wedge & 0_{3 \times 3} \\ -\mathbf{v}^\wedge & -\boldsymbol{\omega}^\wedge \end{bmatrix} \in \mathbb{R}^{6 \times 6}. \quad (7)$$

The coupled kinematics of the spacecraft in the ECI coordinate system can be expressed as

$$\begin{cases} \dot{\mathbf{R}} = \mathbf{R}\boldsymbol{\omega}^\wedge, \\ \dot{\mathbf{b}} = \mathbf{R}\mathbf{v}. \end{cases} \quad (8)$$

The above kinematics equation can be simplified as follows:

$$\dot{\mathbf{g}} = \mathbf{g}\xi^\wedge. \quad (9)$$

The coupled dynamics of the spacecraft in the body-fixed frame can be expressed as

$$\begin{cases} m\dot{\mathbf{v}} + m\boldsymbol{\omega} \times \mathbf{v} = \mathbf{F}_g(\mathbf{b}, \mathbf{R}) + m\mathbf{R}^T \mathbf{a}_{J_2}(\mathbf{b}) + \mathbf{F}_c(\mathbf{b}, \mathbf{R}, \mathbf{v}, \boldsymbol{\omega}) + \mathbf{F}_d, \\ \mathbf{J}\dot{\boldsymbol{\omega}} + \boldsymbol{\omega} \times \mathbf{J}\boldsymbol{\omega} = \mathbf{M}_g(\mathbf{b}, \mathbf{R}) + \mathbf{M}_c(\mathbf{b}, \mathbf{R}, \mathbf{v}, \boldsymbol{\omega}) + \mathbf{M}_d. \end{cases} \quad (10)$$

where m and \mathbf{J} are the mass and moment of inertia of the spacecraft, respectively; \mathbf{F}_g and \mathbf{M}_g are the gravity gradient force and the gravity gradient moment of the spacecraft, respectively; \mathbf{a}_{J_2} is the perturbation caused by the Earth's oblateness; \mathbf{F}_c and \mathbf{M}_c are the control force and control torque of the spacecraft, respectively; and \mathbf{F}_d and \mathbf{M}_d are the unknown external force and external torque caused by radiation pressure, atmosphere drag, and other bounded uncertain disturbances, respectively. The specific forms of \mathbf{F}_g , \mathbf{M}_g , and \mathbf{a}_{J_2} are as follows:

$$\begin{aligned} \mathbf{F}_g &= -\frac{m\mu}{\|\mathbf{b}\|^3} \left[\mathbf{I}_3 + \frac{3}{m\|\mathbf{b}\|^2} \left(\frac{1}{2} \text{tr}(\mathbf{J})\mathbf{I}_3 + \mathbf{J} - \frac{5\mathbf{b}^T \mathbf{R} \mathbf{J} \mathbf{R}^T \mathbf{b}}{2\|\mathbf{b}\|^2} \mathbf{I}_3 \right) \right] \mathbf{R}^T \mathbf{b}, \\ \mathbf{a}_{J_2} &= -\frac{3\mu J_2 \mathbf{R}_e^2}{2\|\mathbf{b}\|^5} \left[\mathbf{b}_x \left(1 - \frac{5\mathbf{b}_z^2}{\|\mathbf{b}\|^2} \right) \mathbf{b}_y \left(1 - \frac{5\mathbf{b}_z^2}{\|\mathbf{b}\|^2} \right) \mathbf{b}_z \left(3 - \frac{5\mathbf{b}_z^2}{\|\mathbf{b}\|^2} \right) \right]^T, \\ \mathbf{M}_g &= \frac{3\mu}{\|\mathbf{b}\|^5} (\mathbf{R}^T \mathbf{b})^\wedge \mathbf{J} \mathbf{R}^T \mathbf{b}, \end{aligned} \quad (11)$$

where $\mu = 398,600.44 \text{ km}^3 \text{ s}^{-2}$ is the gravitational constant of the Earth, $J_2 = 0.00108263$ is the perturbation caused by the Earth's oblateness, and $\mathbf{R}_e = 6378.14 \text{ km}$ is the equatorial radius of the Earth.

Then, the coupling dynamics of the spacecraft can be expressed in a compact form as follows:

$$\Xi = \text{ad}_\xi^* \xi + \Gamma_g + \Gamma_c + \Gamma_d, \quad (12)$$

where $\Xi = \text{diag}(m\mathbf{I}_3, \mathbf{J})$ is the unified inertia matrix of spacecraft, $\Gamma_c = [\mathbf{F}_c^T \ \mathbf{M}_c^T]^T$ is the unified control input vector, and $\Gamma_g = [(\mathbf{F}_g + m\mathbf{R}^T \mathbf{a}_{J_2})^T \ \mathbf{M}_g^T]^T$ is the unified input vector related to gravity.

Thus, combining equations (9) and (12), the coupled kinematics and dynamics of the spacecraft can be expressed compactly as

$$\begin{cases} \dot{\mathbf{g}} = \mathbf{g}\xi^\wedge, \\ \Xi \dot{\xi} = \text{ad}_\xi^* \Xi \xi + \Gamma_g + \Gamma_c + \Gamma_d. \end{cases} \quad (13)$$

Next, based on the above equations, the coupled relative motion tracking error dynamics will be derived. Let \mathbf{g}_o be the actual pose configuration of the leader spacecraft, which the leader spacecraft can be real or virtual; \mathbf{g}_b be the actual pose configuration of the follower spacecraft. Then the actual relative pose configuration between the leader-follower spacecraft is as follows:

$$\mathbf{h} = \mathbf{g}_o^{-1} \mathbf{g}_b. \quad (14)$$

Let \mathbf{g}_d be the desired pose configuration of the leader spacecraft, then the desired relative pose configuration between the leader-follower spacecraft is

$$\mathbf{h}_d = \mathbf{g}_o^{-1} \mathbf{g}_d. \quad (15)$$

Thus the pose configuration tracking error is as follows:

$$\mathbf{h}_e = \mathbf{h}_d^{-1} \mathbf{h} = \mathbf{g}_d^{-1} \mathbf{g}_o \mathbf{g}_o^{-1} \mathbf{g}_b = \mathbf{g}_d^{-1} \mathbf{g}_b. \quad (16)$$

In general, the desired relative pose configuration is a constant value, and the desired relative linear velocity and angular velocity are zero, which means that the follower spacecraft and the leader spacecraft keep relatively stationary in a fixed configuration.

The configuration tracking error of the follower spacecraft can be expressed by exponential coordinates as

$$\boldsymbol{\eta}_e = \begin{bmatrix} \boldsymbol{\rho}_e \\ \boldsymbol{\varphi}_e \end{bmatrix} \in \mathbb{R}^6. \quad (17)$$

The velocity tracking error of the follower spacecraft can be expressed by exponential coordinates as

$$\xi_e = \begin{bmatrix} \mathbf{v}_e \\ \boldsymbol{\omega}_e \end{bmatrix} \in \mathbb{R}^6. \quad (18)$$

Then \mathbf{h}_e can be expressed on SE(3) as

$$\mathbf{h}_e = \begin{bmatrix} \mathbf{R}_e & \mathbf{b}_e \\ 0_{1 \times 3} & 1 \end{bmatrix}. \quad (19)$$

Through the logarithm mapping between the Lie group SE(3) and the Lie algebra $\mathfrak{ce}(3)$, we can get the following results:

$$\begin{aligned} \boldsymbol{\eta}_e &= (\log(\mathbf{h}_e))^\vee, \\ \log(\mathbf{h}_e) &= \begin{bmatrix} \boldsymbol{\varphi}_e^\wedge & \boldsymbol{\rho}_e \\ \mathbf{0}_{1 \times 3} & 0 \end{bmatrix}, \end{aligned} \quad (20)$$

where $\boldsymbol{\rho}_e$ is the position tracking error and $\boldsymbol{\varphi}_e$ is the attitude tracking error, which are expressed as follows:

$$\begin{aligned} \boldsymbol{\rho}_e &= \mathbf{S}^{-1}(\boldsymbol{\varphi}_e) \mathbf{b}_e, \\ \boldsymbol{\varphi}_e^\wedge &= \begin{cases} 0, & \theta = 0, \\ \frac{\theta}{\sin \theta} (\mathbf{R}_e - \mathbf{R}_e^T), & \theta \in (-\pi, \pi), \theta \neq 0, \end{cases} \end{aligned} \quad (21)$$

$$\mathbf{S}^{-1}(\boldsymbol{\varphi}_e) = \mathbf{I} - \frac{1}{2} \boldsymbol{\varphi}_e^\wedge + \frac{1}{\theta^2} \left(1 - \frac{\theta \sin \theta}{2(1 - \cos \theta)} \right) (\boldsymbol{\varphi}_e^\wedge)^2,$$

where $\theta = \arccos((1/2)[\text{tr}(\mathbf{R}_e) - 1])$, which is the norm of $\boldsymbol{\varphi}_e$ and corresponds to the principal rotation angle. When $\theta = 0$, it is injective; when $|\theta| < \pi$, it is bijective.

According to the relationship between Lie group and Lie algebra, it can be deduced that when the desired relative velocity is zero, the expressions of the relative velocity error and relative acceleration error of the follower spacecraft are

$$\begin{aligned} \boldsymbol{\xi}_e &= \boldsymbol{\xi}_b - \text{Ad}_{\mathbf{h}_e^{-1}} \boldsymbol{\xi}_d = \boldsymbol{\xi}_b - \text{Ad}_{\mathbf{h}^{-1}} \boldsymbol{\xi}_o, \\ \dot{\boldsymbol{\xi}}_e &= \dot{\boldsymbol{\xi}}_b + \text{ad}_{\boldsymbol{\xi}_e} \text{Ad}_{\mathbf{h}^{-1}} \boldsymbol{\xi}_o - \text{Ad}_{\mathbf{h}^{-1}} \dot{\boldsymbol{\xi}}_o. \end{aligned} \quad (22)$$

Then the coupled relative motion tracking error kinematics as given in [32] is

$$\dot{\boldsymbol{\eta}}_e = \mathbf{G}(\boldsymbol{\eta}_e) \boldsymbol{\xi}_e, \quad (23)$$

where $\mathbf{G}(\boldsymbol{\eta}_e)$ is expressed as a block-triangular matrix:

$$\mathbf{G}(\boldsymbol{\eta}_e) = \begin{bmatrix} \mathbf{A}(\boldsymbol{\varphi}_e) & \mathbf{T}(\boldsymbol{\varphi}_e, \boldsymbol{\rho}_e) \\ \mathbf{0}_{3 \times 3} & \mathbf{A}(\boldsymbol{\varphi}_e) \end{bmatrix}, \quad (24)$$

where

$$\begin{aligned} \mathbf{A}(\boldsymbol{\varphi}_e) &= \mathbf{I}_3 + \frac{1}{2} \boldsymbol{\varphi}_e^\wedge + \frac{1}{\theta^2} \left(1 - \frac{(1 + \cos \theta) \theta}{2 \sin \theta} \right) (\boldsymbol{\varphi}_e^\wedge)^2, \\ \mathbf{T}(\boldsymbol{\varphi}_e, \boldsymbol{\rho}_e) &= \frac{1}{2} (\mathbf{S}(\boldsymbol{\varphi}_e) \boldsymbol{\rho}_e)^\wedge \mathbf{A}(\boldsymbol{\varphi}_e) + \frac{1}{\theta^2} \left(1 - \frac{(1 + \cos \theta) \theta}{2 \sin \theta} \right) [\boldsymbol{\varphi}_e \boldsymbol{\rho}_e^T + (\boldsymbol{\varphi}_e^T \boldsymbol{\rho}_e) \mathbf{A}(\boldsymbol{\varphi}_e)] \\ &\quad - \frac{(1 + \cos \theta)(\theta - \sin \theta)}{2\theta \sin^2 \theta} \mathbf{S}(\boldsymbol{\varphi}_e) \boldsymbol{\rho}_e \boldsymbol{\varphi}_e^T + \left[\frac{(1 + \cos \theta)(\theta - \sin \theta)}{2\theta^3 \sin^2 \theta} - \frac{2}{\theta^4} \right] \boldsymbol{\varphi}_e^T \boldsymbol{\rho}_e \boldsymbol{\varphi}_e \boldsymbol{\varphi}_e^T. \end{aligned} \quad (25)$$

Taking equation (12) into equation (22) yields

$$\begin{aligned} \Xi \dot{\boldsymbol{\xi}}_e &= \Xi (\dot{\boldsymbol{\xi}}_b + \text{ad}_{\boldsymbol{\xi}_e} \text{Ad}_{\mathbf{h}^{-1}} \boldsymbol{\xi}_o - \text{Ad}_{\mathbf{h}^{-1}} \dot{\boldsymbol{\xi}}_o) \\ &= \text{ad}_{\boldsymbol{\xi}_b}^* \Xi \boldsymbol{\xi}_b + \Gamma_g + \Gamma_c + \Gamma_d + \Xi (\text{ad}_{\boldsymbol{\xi}_e} \text{Ad}_{\mathbf{h}^{-1}} \boldsymbol{\xi}_o - \text{Ad}_{\mathbf{h}^{-1}} \dot{\boldsymbol{\xi}}_o). \end{aligned} \quad (26)$$

However, in actual space missions, the inertia matrix Ξ is uncertain due to fuel consumption and external disturbances, so the actual inertia matrix Ξ can be expressed as

$$\Xi = \Xi_0 + \Delta \Xi, \quad (27)$$

where Ξ_0 is the nominal part and $\Delta \Xi$ is the uncertainty part. Then the inverse of the inertia matrix can be expressed as

$$\begin{aligned} \Xi^{-1} &= (\Xi_0 + \Delta \Xi)^{-1} = \Xi_0^{-1} + \Delta \tilde{\Xi}, \\ \Delta \tilde{\Xi} &= -\Xi_0^{-1} \Delta \Xi (\mathbf{I}_6 + \Xi_0^{-1} \Delta \Xi) \Xi_0^{-1}. \end{aligned} \quad (28)$$

Therefore, (26) can be rewritten as

$$\begin{aligned} \dot{\boldsymbol{\xi}}_e &= \mathbf{H} + \Gamma_0^{-1} \Gamma_c + \Delta \mathbf{d}, \\ \mathbf{H} &= \Gamma_0^{-1} \text{ad}_{\boldsymbol{\xi}_b}^* \Gamma_0 \boldsymbol{\xi}_b + \text{ad}_{\boldsymbol{\xi}_b} \text{Ad}_{\mathbf{h}^{-1}} \boldsymbol{\xi}_o - \text{Ad}_{\mathbf{h}^{-1}} \dot{\boldsymbol{\xi}}_o + \Gamma_0^{-1} \Gamma_g, \\ \Delta \mathbf{d} &= \Delta \tilde{\Xi} (\text{ad}_{\boldsymbol{\xi}_b}^* (\Gamma_0 + \Delta \Gamma) \boldsymbol{\xi}_b + \Gamma_g + \Gamma_c) + \Gamma_0^{-1} \text{ad}_{\boldsymbol{\xi}_b}^* \Delta \Gamma \boldsymbol{\xi}_b + (\Gamma_0^{-1} + \Delta \tilde{\Xi}) \Gamma_d, \end{aligned} \quad (29)$$

where \mathbf{H} is a known deterministic term of the system and $\Delta \mathbf{d}$ is the lumped disturbances, including uncertainties and external disturbances. Then the coupling model of relative motion spacecraft can be expressed as follows:

$$\begin{cases} \dot{\boldsymbol{\eta}}_e = \mathbf{G}(\boldsymbol{\eta}_e) \boldsymbol{\xi}_e, \\ \dot{\boldsymbol{\xi}}_e = \mathbf{H} + \Gamma_0^{-1} \Gamma_c + \Delta \mathbf{d}. \end{cases} \quad (30)$$

2.3. Actuator Configuration with Faults. In this paper, the actuator of attitude control is reaction flywheel, and the actuator of orbit control is thruster. 4 reaction flywheels and 4 pairs of thrusters are used. Then the control vector can be expressed as

$$\Gamma_c = \begin{bmatrix} \mathbf{F}_c \\ \mathbf{M}_c \end{bmatrix} = \mathbf{D} \mathbf{u}, \quad (31)$$

where $\mathbf{D} \in \mathbb{R}^{6 \times 12}$ is the configuration matrix, $\mathbf{u} = [u_1, u_2, u_3, \dots, u_{12}]^T$ is the actual control vector, and u_i ($i = 1, 2, 3, \dots, 12$) is the torque or force that each flywheel or thruster can provide.

The four reaction flywheels adopt the traditional installation method of three orthogonal and one inclined

installation, and the configuration structure is shown in Figure 2.

The control torque distribution matrix of the reaction flywheel is

$$\mathbf{D}_1 = \begin{bmatrix} 1 & 0 & 0 & \frac{\sqrt{3}}{3} \\ 0 & 1 & 0 & \frac{\sqrt{3}}{3} \\ 0 & 0 & 1 & \frac{\sqrt{3}}{3} \end{bmatrix}. \quad (32)$$

Eight thrusters are installed symmetrically at the middle point of each edge of the cube in pairs. The installation mode

of thrust passing through the center of mass is adopted. The configuration structure is shown in Figure 3.

The control force distribution matrix of the thruster is

$$\mathbf{D}_2 = \begin{bmatrix} \frac{\sqrt{2}}{2} & -\frac{\sqrt{2}}{2} & -\frac{\sqrt{2}}{2} & \frac{\sqrt{2}}{2} & -\frac{\sqrt{2}}{2} & \frac{\sqrt{2}}{2} & -\frac{\sqrt{2}}{2} & \frac{\sqrt{2}}{2} \\ 0 & 0 & 0 & 0 & -\frac{\sqrt{2}}{2} & \frac{\sqrt{2}}{2} & \frac{\sqrt{2}}{2} & -\frac{\sqrt{2}}{2} \\ \frac{\sqrt{2}}{2} & -\frac{\sqrt{2}}{2} & \frac{\sqrt{2}}{2} & -\frac{\sqrt{2}}{2} & 0 & 0 & 0 & 0 \end{bmatrix}. \quad (33)$$

Then the attitude and position coupling integrated control distribution matrix \mathbf{D} is

$$\mathbf{D} = \begin{bmatrix} \frac{\sqrt{2}}{2} & -\frac{\sqrt{2}}{2} & -\frac{\sqrt{2}}{2} & \frac{\sqrt{2}}{2} & -\frac{\sqrt{2}}{2} & \frac{\sqrt{2}}{2} & -\frac{\sqrt{2}}{2} & \frac{\sqrt{2}}{2} & 0 & 0 & 0 & 0 \\ 0 & 0 & 0 & 0 & -\frac{\sqrt{2}}{2} & \frac{\sqrt{2}}{2} & \frac{\sqrt{2}}{2} & -\frac{\sqrt{2}}{2} & 0 & 0 & 0 & 0 \\ \frac{\sqrt{2}}{2} & -\frac{\sqrt{2}}{2} & \frac{\sqrt{2}}{2} & -\frac{\sqrt{2}}{2} & 0 & 0 & 0 & 0 & 0 & 0 & 0 & 0 \\ 0 & 0 & 0 & 0 & 0 & 0 & 0 & 0 & 1 & 0 & 0 & \frac{\sqrt{3}}{3} \\ 0 & 0 & 0 & 0 & 0 & 0 & 0 & 0 & 0 & 1 & 0 & \frac{\sqrt{3}}{3} \\ 0 & 0 & 0 & 0 & 0 & 0 & 0 & 0 & 0 & 0 & 1 & \frac{\sqrt{3}}{3} \end{bmatrix}. \quad (34)$$

According to the cause of the faults of the actuator, the failure of the actuator can be divided into the following categories: stuck, loose, saturated, damaged, or invalid. The abovementioned faults types can be unified as follows:

$$\mathbf{u}(t) = \mathbf{E}\mathbf{u}_c(t) + (\mathbf{I} - \mathbf{E})\bar{\mathbf{u}}, \quad (35)$$

where $\mathbf{u}_c(t)$ is the control command of the actuator; $\bar{\mathbf{u}}$ is the stuck fault of the actuator with bounded value and satisfies the constraint $|\bar{u}_i| \leq \min\{u_{i\max}, |u_{i\min}|\}$; $\bar{u}_i = \{u_{i\max}, u_{i\min}\}$ indicates that the i -th thruster is in saturated state; $\bar{u}_i = 0$ indicates that the i -th thruster is in loose position. $\mathbf{E} = \text{diag}(\sigma_1, \sigma_2, \sigma_3, \dots, \sigma_n)$ is the actuator effectiveness matrix and satisfies the constraint $0 \leq \sigma_i \leq 1$. $\sigma_i = 0$ denotes that the i th actuator does not supply any control output; $\sigma_i = 1$ means there is no fault for the i th actuator; and $0 < \sigma_i < 1$ implies the i th actuator has partially lost its effectiveness [38].

Taking equations (31) and (35) into equation (30), the integrated dynamic equation of relative motion spacecraft considering actuator fault can be expressed as follows:

$$\dot{\xi}_e = \mathbf{H} + \Gamma_0^{-1} \mathbf{D}\mathbf{E}\mathbf{u}_c + \Delta\tilde{\mathbf{d}}, \quad (36)$$

where $\Delta\tilde{\mathbf{d}} = \Xi_0^{-1} [\mathbf{D}(\mathbf{I} - \mathbf{E})\bar{\mathbf{u}}] + \Delta\mathbf{d}$.

3. Adaptive Fuzzy Modified Fixed-Time Fault-Tolerant Controller Design and Stability Analysis

In this part, our goal is to design a fault-tolerant controller on the relative coupled dynamics so that the configuration of the spacecraft can converge to the desired state in the presence of model uncertainties and external disturbances and actuator faults in fixed time.

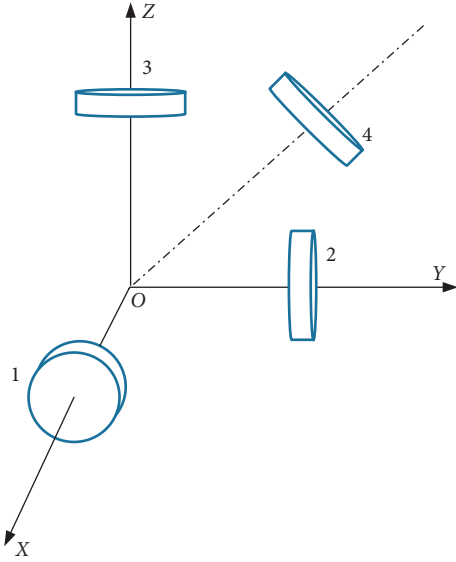


FIGURE 2: Configuration structure of flywheels.

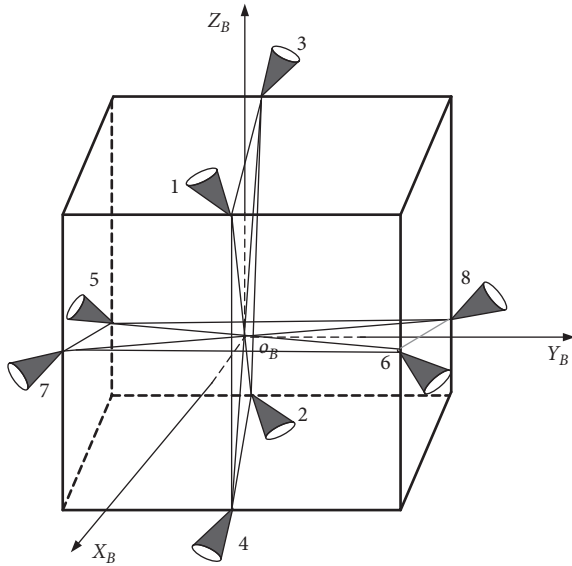


FIGURE 3: Configuration structure of thrusters.

3.1. Introduction of Fuzzy Approximation Technique. The spacecraft exhibits strong nonlinearity due to the influence of lumped disturbances, which will affect the performance of the controller. So it is critical to approximate the lumped disturbances with high accuracy, and fuzzy logic system (FLS) is an effective way to realize this objective. The fuzzy approximation method can make full use of fuzzy linguistic information to approximate any nonlinear continuous function. It has a good effect in fitting nonlinear function. It can approach nonlinear continuous function with arbitrary precision. The structure and basic theory of fuzzy approximation system are given below [32].

$\mathbf{X} = (x_1, x_2, \dots, x_n)^T \in \mathbb{R}^n$ is the input variable of the FLS, and M fuzzy rules are designed for each component of

the input variable, then the whole system has n^M fuzzy rules, and the specific expression of each fuzzy rule is

$$\text{IF } x_1 \text{ is } A_1^l \text{ and } \dots \text{ and } x_N \text{ is } A_N^l \text{ THEN } z \text{ is } B^l, \quad (37)$$

where $l_i = 1, \dots, M$ is the number of fuzzy rules for each input variable x_k , z is the output of the fuzzy system, A_k^l is the fuzzy set of system input variables, and B^l is the fuzzy set of system output.

If the fuzzy system adopts singleton fuzzifier, center-average defuzzifier, and product inference engine, the output of fuzzy approximation system can be obtained as follows:

$$z = \frac{\bar{z}^l \left(\prod_{k=1}^N \mu_{A_k^l}(x_k) \right)}{\sum_{l=1}^M \left(\prod_{k=1}^N \mu_{A_k^l}(x_k) \right)}, \quad (38)$$

where $\mu_{A_k^l}(x_k)$ is the membership function corresponding to the input variable x_k ; in this paper, Gauss membership function is used with the form

$$\mu_{A_k^l}(x_k) = a_k^l \exp\left(-\frac{1}{2} \left(\frac{x_k - \bar{x}_k^l}{b_k^l}\right)^2\right), \quad (39)$$

where a_k^l, \bar{x}_k^l , and b_k^l are all positive real parameters with $0 < a_k^l \leq 1$. \bar{x}_k^l is the abscissa corresponding to the membership function $\mu_{A_k^l}(x_k)$ when the maximum value is 1.

Let $\mathbf{W} = (\bar{z}^1, \bar{z}^2, \dots, \bar{z}^M)$, then equation (38) can be rewritten as follows:

$$z = \mathbf{W}\boldsymbol{\beta}, \quad (40)$$

where $\boldsymbol{\beta}$ is the basis function, which can be expressed as

$$\boldsymbol{\beta}(\mathbf{X}) = \frac{\prod_{k=1}^N \mu_{A_k^l}(x_k)}{\sum_{l=1}^M \left(\prod_{k=1}^N \mu_{A_k^l}(x_k) \right)}. \quad (41)$$

Based on the above introduction, the total external disturbances of the follower spacecraft can be estimated by the fuzzy approximation as

$$\Delta \tilde{d} = \mathbf{W}^* \boldsymbol{\beta}(\mathbf{X}) + \boldsymbol{\varepsilon}, \quad (42)$$

where \mathbf{W}^* is the optimal weight matrix and $\boldsymbol{\varepsilon}$ is the bounded approximation error of FLS. Let $\tilde{\mathbf{W}}$ be the estimation of \mathbf{W}^* . The sliding surface \mathbf{S} is the input variable of $\boldsymbol{\beta}(\mathbf{X})$, and then the estimated value $\Delta \tilde{d}$ of the total external disturbances $\Delta \tilde{d}$ of the spacecraft can be expressed as

$$\Delta \tilde{d} = \tilde{\mathbf{W}} \boldsymbol{\beta}(\mathbf{X}) + \boldsymbol{\varepsilon}. \quad (43)$$

Then the estimation error of the optimal weight matrix is

$$\tilde{\mathbf{W}} = \tilde{\mathbf{W}} - \mathbf{W}^*. \quad (44)$$

In order to design and analyze the controller, some assumptions are given below.

Assumption 1. The output of FLS is bounded, and the estimated value of the external total disturbances is bounded such that

$$\|\widehat{\Delta d}\| \leq d_m, \quad (45)$$

where d_m is a positive constant.

Assumption 2. The approximation error of FLS is bounded such that

$$\|\boldsymbol{\varepsilon}\| \leq \varepsilon_m, \quad (46)$$

where ε_m is a positive constant.

Assumption 3. The optimal weight matrix of FLS is bounded such that

$$\text{tr}(\widetilde{W}^T \widetilde{W}) \leq W_m, \quad (47)$$

where W_m is a positive constant.

Assumption 4. The faults of the actuators satisfy the constraint $\text{rank}(\mathbf{DE}) = 6$, and this means that the redundant actuators can still combine enough control output to complete the given goal.

Remark 1. Because the mass, moment of inertia, fault amplitude, input variables of FLS, and external disturbance of the system are bounded, so Assumption 1 is reasonable; Assumptions 2 and 3 have the property that fuzzy approximation system can fit any nonlinear continuous function, and Assumption 4 does not consider under-actuated system, so it is also reasonable.

3.2. Controller Design. In order to achieve the control goal of modified fixed time stability, 3 sliding surface forms are proposed as follows.

Firstly, the finite-time terminal sliding mode is denoted as

$$\mathbf{S} = \boldsymbol{\xi}_e + \mathbf{C}_1 \boldsymbol{\eta}_e + \mathbf{C}_2 \text{sig}^\alpha(\boldsymbol{\eta}_e). \quad (48)$$

Then, the fixed-time terminal sliding mode is denoted as

$$\mathbf{S} = \boldsymbol{\xi}_e + \mathbf{C}_1 \text{sig}^{\alpha_1}(\boldsymbol{\eta}_e) + \mathbf{C}_2 \text{sig}^{\alpha_2}(\boldsymbol{\eta}_e). \quad (49)$$

Finally, the modified fixed-time terminal sliding mode is denoted as

$$\mathbf{S} = \boldsymbol{\xi}_e + \mathbf{C}_1 \text{sig}^{(1/2)+(1/2)\alpha_1+(1/2)\alpha_1-(1/2)\text{sgn}(|\boldsymbol{\eta}_e|-1)}(\boldsymbol{\eta}_e) + \mathbf{C}_2 \text{sig}^{\alpha_2}(\boldsymbol{\eta}_e), \quad (50)$$

where $\mathbf{C}_1, \mathbf{C}_2 \in \mathbb{R}^{6 \times 6}$ are both positive definite diagonal matrices, $\alpha \in ((1/2), 1)$, and $\alpha_1 \in (1, +\infty)$, $\alpha_2 \in ((1/2), 1)$.

Remark 2. In fact, equation (50) is developed on the basis of equations (49) and (48), and it can be classified and discussed as follows:

- (1) When $|\eta_e| < 1$, equation (50) can be expressed as $\mathbf{S} = \boldsymbol{\xi}_e + \mathbf{C}_1 |\eta_e| \text{sgn}(\eta_e) + \mathbf{C}_2 \text{sig}^\alpha(\eta_e)$, and it has a similar form to equation (48).
- (2) When $|\eta_e| = 1$, equation (50) can be expressed as $\mathbf{S} = \boldsymbol{\xi}_e + \mathbf{C}_1 \text{sig}^{(1/2)+(1/2)\alpha_1}(\eta_e) + \mathbf{C}_2 \text{sig}^{\alpha_2}(\eta_e)$, and it has a similar form to equation (49).
- (3) When $|\eta_e| > 1$, equation (50) can be expressed as $\mathbf{S} = \boldsymbol{\xi}_e + \mathbf{C}_1 \text{sig}^{\alpha_1}(\eta_e) + \mathbf{C}_2 \text{sig}^{\alpha_2}(\eta_e)$, and it has the same form to equation (49).

From the above analysis and discussion, we can see that the modified fixed-time terminal sliding mode is a combination of the finite-time terminal sliding mode and the fixed-time terminal sliding mode under different conditions. To guarantee that the relative motion can spacecraft converge to the desired state in the expected time even in the case of actuator faults, the corresponding three kinds of adaptive fuzzy sliding mode controllers are designed as follows:

- (1) Corresponding to (48), adaptive fuzzy finite-time fault-tolerant controller (AF-Finite) is given as

$$\mathbf{u}_c = -(\mathbf{DE})^\dagger \left\{ \Gamma_0 (\mathbf{H} + \mathbf{C}_1 \mathbf{G}(\boldsymbol{\eta}_e) \boldsymbol{\xi}_e + \alpha \mathbf{C}_2 \text{diag}(|\boldsymbol{\eta}_e|^{\alpha-1}) \mathbf{G}(\boldsymbol{\eta}_e) \boldsymbol{\xi}_e + \widehat{W} \boldsymbol{\beta}(\mathbf{X})) + \mathbf{K}_1 \mathbf{S} + \mathbf{K}_2 \text{sig}^\alpha(\mathbf{S}) \right\}. \quad (51)$$

- (2) Corresponding to (49), adaptive fuzzy fixed-time fault-tolerant controller (AF-Fixed) is given as

$$\mathbf{u}_c = -(\mathbf{DE})^\dagger \left\{ \Gamma_0 \left(\begin{array}{l} \mathbf{H} + \alpha_1 \mathbf{C}_1 \text{diag}(|\boldsymbol{\eta}_e|^{\alpha_1-1}) \mathbf{G}(\boldsymbol{\eta}_e) \boldsymbol{\xi}_e + \\ \alpha_2 \mathbf{C}_2 \text{diag}(|\boldsymbol{\eta}_e|^{\alpha_2-1}) \mathbf{G}(\boldsymbol{\eta}_e) \boldsymbol{\xi}_e + \widehat{W} \boldsymbol{\beta}(\mathbf{X}) \end{array} \right) + \mathbf{K}_1 \text{sig}^{\alpha_1}(\mathbf{S}) + \mathbf{K}_2 \text{sig}^{\alpha_2}(\mathbf{S}) \right\}. \quad (52)$$

- (3) Corresponding to (50), adaptive fuzzy modified fixed-time fault-tolerant controller (AF-MFixed) is given as

$$\mathbf{u}_c = -(\mathbf{DE})^\dagger \left\{ \Gamma_0 \left(\begin{array}{l} \left(\frac{1+\alpha_1}{2} + \frac{\alpha_1-1}{2} \operatorname{sgn}(|\boldsymbol{\eta}_e| - 1) \right) \mathbf{C}_1 \operatorname{diag} \left(|\boldsymbol{\eta}_e|^{((1+\alpha_1/2)+(\alpha_1-1/2)\operatorname{sgn}(|\boldsymbol{\eta}_e|-1))^{-1}} \right) \mathbf{G}(\boldsymbol{\eta}_e) \boldsymbol{\xi}_e \\ + \alpha_2 \mathbf{C}_2 \operatorname{diag} \left(|\boldsymbol{\eta}_e|^{\alpha_2-1} \right) \mathbf{G}(\boldsymbol{\eta}_e) \boldsymbol{\xi}_e + \widehat{\mathbf{W}} \boldsymbol{\beta}(\mathbf{X}) + \mathbf{H} \\ + \mathbf{K}_1 \operatorname{sig}^{(1+\alpha_1/2)+(\alpha_1-1/2)\operatorname{sgn}(|\mathbf{S}|-1)}(\mathbf{S}) + \mathbf{K}_2 \operatorname{sig}^{\alpha_2}(\mathbf{S}) \end{array} \right) \right\}, \quad (53)$$

where $(\mathbf{DE})^\dagger = (\mathbf{DE})^T [(\mathbf{DE})(\mathbf{DE})^T]^{-1}$ is the pseudoinverse of matrix \mathbf{DE} ; from Assumption 4, we know that $\mathbf{DE}(\mathbf{DE})^T$ is full rank, so its pseudoinverse exists; $\mathbf{K}_1, \mathbf{K}_2 \in \mathbb{R}^{6 \times 6}$ are both positive definite diagonal matrices.

Then the adaptive update law of the optimal weight matrix $\widehat{\mathbf{W}}$ is given by

$$\dot{\widehat{\mathbf{W}}} = \dot{\widetilde{\mathbf{W}}} = \gamma \Gamma_0^T \mathbf{S} \boldsymbol{\beta}^T(\mathbf{X}), \quad (54)$$

where $\gamma > 0$ is an auxiliary parameter independent of control.

3.3. Stability Analysis. In this part, we will take the stability proof of AF-finite fault-tolerant controller as an example for stability analysis, and the other two (AF-Fixed and AF-MFixed) stability analysis methods are the same as is. Some lemmas are given before the stability analysis.

Lemma 1 (see [6]). *Assuming that $V(\mathbf{x}): \mathbb{R}^n \rightarrow \mathbb{R}$ is a continuous positive definite function and satisfies the following differential inequality*

$$\dot{V}(\mathbf{x}) + \rho_1 V(\mathbf{x}) + \rho_2 V^v(\mathbf{x}) \leq 0, \quad \forall t > 0, \quad (55)$$

where $\rho_1 > 0, \rho_2 > 0, v \in (0, 1)$, then $V(\mathbf{x})$ can converge to the equilibrium point in finite time, and the finite time T satisfies the following constraints:

$$T \leq \frac{1}{\rho_1(1-v)} \ln \frac{\rho_1 V^{1-v}(\mathbf{x}_0) + \rho_2}{\rho_2}. \quad (56)$$

Lemma 2 (see [38]). *Assuming that $V(\mathbf{x}): \mathbb{R}^n \rightarrow \mathbb{R}$ is a continuous positive definite function and satisfies the following differential inequality:*

$$\dot{V}(\mathbf{x}) + \rho_1 V^{v_1}(\mathbf{x}) + \rho_2 V^{v_2}(\mathbf{x}) \leq 0, \quad \forall t > 0, \quad (57)$$

where $\rho_1 > 0, \rho_2 > 0, v_1 > 1, v_2 \in (0, 1)$, then $V(\mathbf{x})$ can converge to the equilibrium point in fixed time, and the fixed time T satisfies the following constraints:

$$T \leq \frac{1}{\rho_1(v_1-1)} + \frac{1}{\rho_2(1-v_2)}. \quad (58)$$

Lemma 3 (see [3]). *Assuming that $V(\mathbf{x}): \mathbb{R}^n \rightarrow \mathbb{R}$ is a continuous positive definite function and satisfies the following differential inequality*

$$\dot{V}(\mathbf{x}) + \rho_1 V^{(1/2)+(1/2)v_1+(1/2)v_1-(1/2)\operatorname{sgn}(V(\mathbf{x})-1)}(\mathbf{x}) + \rho_2 V^{v_2}(\mathbf{x}) \leq 0, \quad \forall t > 0, \quad (59)$$

where $\rho_1 > 0, \rho_2 > 0, v_1 > 1, v_2 \in (0, 1)$, then $V(\mathbf{x})$ can converge to the equilibrium point in modified fixed time, and the modified fixed time T satisfies the following constraints:

$$T \leq \frac{1}{\rho_1(v_1-1)} + \frac{1}{\rho_2(1-v_2)} \ln \left(1 + \frac{\rho_1}{\rho_2} \right). \quad (60)$$

Because the inequality $\ln(1 + (\rho_1/\rho_2)) \leq (\rho_1/\rho_2)$ holds, the convergence time in Lemma 3 is shorter than that in Lemma 2.

Lemma 4 (see [32]). The eigenvalues of matrix $\mathbf{G}(\boldsymbol{\eta}_e)$ are all positive.

Next, the Lyapunov method will be used to prove the reachability of sliding mode variables and the convergence of the system states.

Theorem 1. *When the nonlinear system equation (48) reaches the sliding mode surface $\mathbf{S} = 0$, the state $\boldsymbol{\eta}_e, \boldsymbol{\xi}_e$ of the system can converge to the equilibrium point in a finite time.*

Proof. When equation (48) reaches the sliding mode surface $\mathbf{S} = 0$, such that

$$\mathbf{S} = \boldsymbol{\xi}_e + \mathbf{C}_1 \boldsymbol{\eta}_e + \mathbf{C}_2 \operatorname{sig}^\alpha(\boldsymbol{\eta}_e) = 0, \quad (61)$$

then we have

$$\boldsymbol{\xi}_e = -\mathbf{C}_1 \boldsymbol{\eta}_e - \mathbf{C}_2 \operatorname{sig}^\alpha(\boldsymbol{\eta}_e). \quad (62)$$

A candidate Lyapunov function is selected as follows:

$$V = \frac{1}{2} \boldsymbol{\eta}_e^T \boldsymbol{\eta}_e. \quad (63)$$

Taking the derivative of V with respect to time yields:

$$\begin{aligned}\dot{V} &= \boldsymbol{\eta}_e^T \dot{\boldsymbol{\eta}}_e = \boldsymbol{\eta}_e^T \mathbf{G}(\boldsymbol{\eta}_e) \boldsymbol{\xi}_e = \boldsymbol{\eta}_e^T \mathbf{G}(\boldsymbol{\eta}_e) [-\mathbf{C}_1 \boldsymbol{\eta}_e - \mathbf{C}_2 \text{sig}^\alpha(\boldsymbol{\eta}_e)] \\ &\leq -\lambda_{\min}(\mathbf{G}(\boldsymbol{\eta}_e) \mathbf{C}_1) \|\boldsymbol{\eta}_e\|_2^2 - \lambda_{\min}(\mathbf{G}(\boldsymbol{\eta}_e) \mathbf{C}_2) \|\boldsymbol{\eta}_e\|^{1+\alpha} \\ &\leq -2\lambda_{\min}(\mathbf{G}(\boldsymbol{\eta}_e) \mathbf{C}_1) V - 2^{(1+\alpha/2)} \lambda_{\min}(\mathbf{G}(\boldsymbol{\eta}_e) \mathbf{C}_2) V^{(1+\alpha/2)} \\ &= -a_1 V - a_2 V^{(1+\alpha/2)},\end{aligned}\quad (64)$$

where $a_1 = 2\lambda_{\min}(\mathbf{G}(\boldsymbol{\eta}_e) \mathbf{C}_1)$, $a_2 = 2^{(1+\alpha/2)} \lambda_{\min}(\mathbf{G}(\boldsymbol{\eta}_e) \mathbf{C}_2)$, by using Lemma 4 we know that the eigenvalues of matrix $\mathbf{G}(\boldsymbol{\eta}_e)$ are all positive; in addition, $\mathbf{C}_1, \mathbf{C}_2 \in \mathbb{R}^{6 \times 6}$ are both positive definite diagonal matrices, and then we have $a_1, a_2 > 0$. By using Lemma 1, we can conclude that V will converge to equilibrium point in finite time T , such that

$$T \leq \frac{2}{a_1(1-\alpha)} \ln \left(\frac{a_1 V^{(1-\alpha/2)}(0)}{a_2} + 1 \right). \quad (65)$$

So, $\boldsymbol{\eta}_e$ can also converge to equilibrium point in finite time; according to equation (62), $\boldsymbol{\xi}_e$ will converge to equilibrium point in finite time too. \square

Remark 3. Since $\alpha \mathbf{C}_2 \text{diag}(|\boldsymbol{\eta}_e|^{\alpha-1}) \mathbf{G}(\boldsymbol{\eta}_e) \boldsymbol{\xi}_e$ is included in equation (51), when $\boldsymbol{\eta}_e$ reaches the equilibrium point before $\boldsymbol{\xi}_e$, the control output will become infinite. The singularity can be avoided by selecting $\alpha \in ((1/2), 1)$ in this paper. Because when $\boldsymbol{\eta}_e = 0$, the following equation holds:

$$\begin{aligned}\alpha \mathbf{C}_2 \text{diag}(|\boldsymbol{\eta}_e|^{\alpha-1}) \mathbf{G}(\boldsymbol{\eta}_e) \boldsymbol{\xi}_e &= \alpha \mathbf{C}_2 \text{diag}(|\boldsymbol{\eta}_e|^{\alpha-1}) \mathbf{G}(\boldsymbol{\eta}_e) (-\mathbf{C}_1 \boldsymbol{\eta}_e - \mathbf{C}_2 \text{sig}^\alpha(\boldsymbol{\eta}_e)) \\ &= -\alpha \mathbf{C}_2 \mathbf{C}_1 \mathbf{G}(\boldsymbol{\eta}_e) |\boldsymbol{\eta}_e|^\alpha - \alpha \mathbf{C}_2^2 \mathbf{G}(\boldsymbol{\eta}_e) \text{sig}^{2\alpha-1}(\boldsymbol{\eta}_e) = 0.\end{aligned}\quad (66)$$

Remark 4. When we choose the other two sliding surfaces in equations (49) and (50) and use the same proof method as Theorem 1, we can also get that the system state will converge to the equilibrium point in fixed time. By using equation (49) and Lemma 2, $\boldsymbol{\eta}_e, \boldsymbol{\xi}_e$ will converge to the equilibrium point in fixed time T_f :

$$T_f \leq \frac{2}{a_{1f}(\alpha_1 - 1)} + \frac{2}{a_{2f}(1 - \alpha_2)}, \quad (67)$$

where $a_{1f} = 2^{(1+\alpha_1/2)} \lambda_{\min}(\mathbf{G}(\boldsymbol{\eta}_e) \mathbf{C}_1)$ and $a_{2f} = 2^{(1+\alpha_2/2)} \lambda_{\min}(\mathbf{G}(\boldsymbol{\eta}_e) \mathbf{C}_2)$.

By using equation (50) and Lemma 3, $\boldsymbol{\eta}_e, \boldsymbol{\xi}_e$ will converge to the equilibrium point in modified fixed time T_m :

$$T_m \leq \frac{2}{a_{1m}(\alpha_1 - 1)} + \frac{2}{a_{1m}(1 - \alpha_2)} \ln \left(1 + \frac{a_{1m}}{a_{2m}} \right), \quad (68)$$

where $a_{1m} = 2^{(1+(1/2)+(1/2)\alpha_1 + ((1/2)\alpha_1 - (1/2))\text{sgn}(|\boldsymbol{\eta}_e| - 1/2))} \lambda_{\min}(\mathbf{G}(\boldsymbol{\eta}_e) \mathbf{C}_1)$ and $a_{2m} = 2^{(1+\alpha_2/2)} \lambda_{\min}(\mathbf{G}(\boldsymbol{\eta}_e) \mathbf{C}_2)$.

To guarantee that the sliding surface can reach $\mathbf{S} = 0$ in finite time, Theorem 2 is proposed.

Theorem 2. For the relative motion spacecraft system with actuator faults in equation (36), the sliding surface \mathbf{S} of the system can converge to a small region containing zero in finite time when using sliding surface in equation (48) and fuzzy adaptive control law in equations (51) and (54).

Proof. Another candidate Lyapunov function is selected as follows:

$$V_1 = \frac{1}{2} \mathbf{S}^T \boldsymbol{\Gamma}_0 \mathbf{S} + \frac{1}{2\gamma} \text{tr}(\tilde{\mathbf{W}}^T \tilde{\mathbf{W}}). \quad (69)$$

Taking the derivative of V_1 yields

$$\begin{aligned}\dot{V}_1 &= \mathbf{S}^T \boldsymbol{\Gamma}_0 \dot{\mathbf{S}} + \frac{1}{\gamma} \text{tr}(\tilde{\mathbf{W}}^T \dot{\tilde{\mathbf{W}}}) \\ &= \mathbf{S}^T \boldsymbol{\Gamma}_0 (\dot{\boldsymbol{\xi}}_e + \mathbf{C}_1 \mathbf{G}(\boldsymbol{\eta}_e) \boldsymbol{\xi}_e + \alpha \mathbf{C}_2 \text{diag}(|\boldsymbol{\eta}_e|^{\alpha-1}) \mathbf{G}(\boldsymbol{\eta}_e) \boldsymbol{\xi}_e) + \frac{1}{\gamma} \text{tr}(\tilde{\mathbf{W}}^T \dot{\tilde{\mathbf{W}}}) \\ &= \mathbf{S}^T \boldsymbol{\Gamma}_0 \left(\begin{array}{c} \mathbf{H} + \boldsymbol{\Gamma}_0^{-1} \mathbf{D} \mathbf{E} \mathbf{u}_c + \Delta \tilde{\mathbf{d}} + \mathbf{C}_1 \mathbf{G}(\boldsymbol{\eta}_e) \boldsymbol{\xi}_e \\ + \alpha \mathbf{C}_2 \text{diag}(|\boldsymbol{\eta}_e|^{\alpha-1}) \mathbf{G}(\boldsymbol{\eta}_e) \boldsymbol{\xi}_e \end{array} \right) + \frac{1}{\gamma} \text{tr}(\tilde{\mathbf{W}}^T \dot{\tilde{\mathbf{W}}}) \\ &= -\mathbf{S}^T \boldsymbol{\Gamma}_0 \tilde{\mathbf{W}} \boldsymbol{\beta}(\mathbf{X}) + \mathbf{S}^T \boldsymbol{\Gamma}_0 \boldsymbol{\varepsilon} - \mathbf{S}^T \mathbf{K}_1 \mathbf{S} - \mathbf{S}^T \mathbf{K}_2 \text{sig}^\alpha(\mathbf{S}) + \frac{1}{\gamma} \text{tr}(\tilde{\mathbf{W}}^T \dot{\tilde{\mathbf{W}}}) \\ &= \frac{1}{\gamma} \text{tr}(\tilde{\mathbf{W}}^T (\dot{\tilde{\mathbf{W}}} - \gamma \boldsymbol{\Gamma}_0^T \mathbf{S} \boldsymbol{\beta}^T(\mathbf{X}))) + \mathbf{S}^T \boldsymbol{\Gamma}_0 \boldsymbol{\varepsilon} - \mathbf{S}^T \mathbf{K}_1 \mathbf{S} - \mathbf{S}^T \mathbf{K}_2 \text{sig}^\alpha(\mathbf{S}).\end{aligned}\quad (70)$$

Substituting the adaptive law of equation (54) into the above equation yields

$$\begin{aligned} \dot{V}_1 &= \mathbf{S}^T \Gamma_0 \boldsymbol{\varepsilon} - \mathbf{S}^T \mathbf{K}_1 \mathbf{S} - \mathbf{S}^T \mathbf{K}_2 \text{sig}^\alpha(\mathbf{S}) \\ &\leq -\lambda_{\min}(\mathbf{K}_1) \frac{2}{\lambda_{\max}(\Gamma_0)} \frac{1}{2} \mathbf{S}^T \Gamma_0 \mathbf{S} - \lambda_{\min}(\mathbf{K}_2) \left[\frac{2}{\lambda_{\max}(\Gamma_0)} \right]^{(1+\alpha/2)} \left[\frac{1}{2} \mathbf{S}^T \Gamma_0 \mathbf{S} \right]^{(1+\alpha/2)} \\ &\quad - \frac{1}{2\gamma} \text{tr}(\tilde{\mathbf{W}}^T \tilde{\mathbf{W}}) - \left[\frac{1}{2\gamma} \text{tr}(\tilde{\mathbf{W}}^T \tilde{\mathbf{W}}) \right]^{(1+\alpha/2)} + \Delta, \end{aligned} \quad (71)$$

where Δ is defined as

$$\Delta = \frac{1}{2\gamma} \text{tr}(\tilde{\mathbf{W}}^T \tilde{\mathbf{W}}) + \left[\frac{1}{2\gamma} \text{tr}(\tilde{\mathbf{W}}^T \tilde{\mathbf{W}}) \right]^{(1+\alpha/2)} + \|\mathbf{S}\| \|\Gamma_0\| \|\boldsymbol{\varepsilon}\|. \quad (72)$$

From Assumptions 2 and 3, we know that the following inequalities are satisfied:

$$\Delta \leq \frac{1}{2\gamma} W_m + \left(\frac{1}{2\gamma} W_m \right)^{(1+\alpha/2)} + \varepsilon_m \|\mathbf{S}\| \|\Gamma_0\| = \Delta', \quad (73)$$

where χ_1 and χ_2 are defined to satisfy the following equations:

$$\begin{aligned} \chi_1 &= \min \left\{ \lambda_{\min}(\mathbf{K}_1) \frac{2}{\lambda_{\max}(\Gamma_0)}, 1 \right\}, \\ \chi_2 &= \min \left\{ \lambda_{\min}(\mathbf{K}_2) \left(\frac{2}{\lambda_{\max}(\Gamma_0)} \right)^{(1+\alpha/2)}, 1 \right\}. \end{aligned} \quad (74)$$

Then equation (71) can be simplified as

$$\dot{V}_1 \leq -\chi_1 V_1 - \chi_2 V_1^{(1+\alpha/2)} + \Delta'. \quad (75)$$

The above equation can be rewritten as

$$\begin{cases} \dot{V}_1 + \bar{\chi}_1 V_1 + \chi_2 V_1^{(1+\alpha/2)} \leq 0, \\ \dot{V}_1 + \chi_1 V_1 + \bar{\chi}_2 V_1^{(1+\alpha/2)} \leq 0, \end{cases} \quad (76)$$

where $\bar{\chi}_1 = \chi_1 - (\Delta'/V_1)$ and $\bar{\chi}_2 = \chi_2 - (\Delta'/V_1^{(1+\alpha/2)})$, by using Lemma 1, V_1 will converge to the equilibrium point in finite time.

When $\bar{\chi}_1 > 0$, that is, $V_1 > (\Delta'/\chi_1)$, V_1 will converge to the region Δ_1 containing zero in finite time T_1 :

$$\begin{aligned} T_1 &\leq \frac{2}{\bar{\chi}_1(1-\alpha)} \ln \left(\frac{\bar{\chi}_1 V^{(1-\alpha/2)}(0)}{\chi_2} + 1 \right), \\ \Delta_1 &\leq \frac{\Delta'}{\chi_1}. \end{aligned} \quad (77)$$

When $\bar{\chi}_2 > 0$, that is, $V_1 > (\Delta'/\chi_2)^{(2/1+\alpha)}$, V_1 will converge to the region Δ_2 containing zero in finite time T_2 :

$$\begin{aligned} T_2 &\leq \frac{2}{\chi_1(1-\alpha)} \ln \left(\frac{\chi_1 V^{(2/1-\alpha)}(0)}{\bar{\chi}_2} + 1 \right), \\ \Delta_2 &\leq \left(\frac{\Delta'}{\chi_2} \right)^{(2/1+\alpha)}. \end{aligned} \quad (78)$$

According to equations (77) and (78), we can conclude that V_1 will converge to the region $\bar{\Delta}$ containing zero in finite time T' :

$$\begin{aligned} T' &= \min\{T_1, T_2\}, \\ \bar{\Delta} &= \min\{\Delta_1, \Delta_2\}. \end{aligned} \quad (79)$$

Since the following inequality holds

$$\begin{aligned} \frac{1}{2} \mathbf{S}^T \Gamma_0 \mathbf{S} &\leq V_1, \\ \frac{1}{2\gamma} \text{tr}(\tilde{\mathbf{W}}^T \tilde{\mathbf{W}}) &\leq V_1, \end{aligned} \quad (80)$$

the sliding surface \mathbf{S} of the system can converge to a small region $\Delta_S = \sqrt{(2/\lambda_{\min}(\Xi_0))\bar{\Delta}}$ containing zero in finite time. The estimated value of the optimal weight matrix can also converge to the true value. \square

Remark 5. When we choose the other two controllers in equations (52) and (53) and use the same adaptive update law in equation (54), we can also draw the conclusion that the sliding surface converges in fixed time. By using equation (52) and Lemma 2, V_1 will converge to the region $\bar{\Delta}_f$ containing zero in fixed time T'_f .

$$\begin{aligned} T'_f &= \min\{T_{1f}, T_{2f}\}, \\ \bar{\Delta}_f &= \min\{\Delta_{1f}, \Delta_{2f}\}, \end{aligned} \quad (81)$$

where $T_{1f} \leq (2/\bar{\chi}_{1f}(\alpha_1 - 1)) + (2/\chi_{2f}(1 - \alpha_2))$, $\Delta_{1f} \leq (\Delta'_f/\chi_{1f})^{(2/1+\alpha_1)}$; $T_{2f} \leq (2/\chi_{1f}(\alpha_1 - 1)) + (2/\bar{\chi}_{2f}(1 - \alpha_2))$, $\Delta_{2f} \leq (\Delta'_f/\chi_{2f})^{(2/1+\alpha_2)}$. The derivation process of χ_{1f} , $\bar{\chi}_{1f}$, χ_{2f} , and $\bar{\chi}_{2f}$ can be referenced with Theorem 2.

By using equation (53) and Lemma 3, V_1 will converge to the region $\bar{\Delta}_m$ containing zero in fixed time T'_m :

$$\begin{aligned} T'_m &= \min\{T_{1m}, T_{2m}\}, \\ \bar{\Delta}_m &= \min\{\Delta_{1m}, \Delta_{2m}\}, \end{aligned} \quad (82)$$

where $T_{1m} \leq (2/\bar{\chi}_{1m}(\alpha_1 - 1)) + (2/\chi_{1m}(1 - \alpha_2))\ln(\chi_{1m}/\chi_{2m})$, $\Delta_{1m} \leq (\Delta_m/\chi_{1m})^{(2/1+\alpha_1)}$; $T_{2m} \leq (2/\bar{\chi}_{1m}(\alpha_1 - 1)) + (2/\bar{\chi}_{1m}(1 - \alpha_2))\ln(\bar{\chi}_{1m}/\bar{\chi}_{2m})$, $\Delta_{2m} \leq (\Delta_m/\chi_{2m})^{(2/1+\alpha_2)}$. The derivation process of χ_{1m} , $\bar{\chi}_{1m}$, χ_{2m} , and $\bar{\chi}_{2m}$ can be referenced with Theorem 2.

4. Numerical Simulation Analysis

In this part, three kinds of fuzzy adaptive finite-time and fixed-time fault-tolerant control algorithms proposed in this paper are simulated to verify the effectiveness of the algorithms. Before the simulation, the input expression of the fuzzy approximation system is defined as

$$x_k = \frac{s_k}{|s_k| + 0.0001}, \quad (k = 1, 2, \dots, 6). \quad (83)$$

Seven fuzzy membership functions are selected as follows:

$$\left\{ \begin{array}{l} \mu_{A_k^1}(x_k) = \frac{1}{1 + \exp(5(x_k + \pi/4))}, \\ \mu_{A_k^2}(x_k) = \exp\left(-0.5\left(\frac{x_k + 1}{0.25}\right)^2\right), \\ \mu_{A_k^3}(x_k) = \exp\left(-0.5\left(\frac{x_k + 0.5}{0.25}\right)^2\right), \\ \mu_{A_k^4}(x_k) = \exp\left(-0.5\left(\frac{x_k}{0.25}\right)^2\right), \\ \mu_{A_k^5}(x_k) = \exp\left(-0.5\left(\frac{x_k - 0.5}{0.25}\right)^2\right), \\ \mu_{A_k^6}(x_k) = \exp\left(-0.5\left(\frac{x_k - 1}{0.25}\right)^2\right), \\ \mu_{A_k^7}(x_k) = \frac{1}{1 + \exp(5(x_k - \pi/4))}. \end{array} \right. \quad (84)$$

In the simulation, the mass and moment of inertia of the follower spacecraft and the leader spacecraft are chosen the same as

$$m = 110\text{kg},$$

$$\mathbf{J} = \begin{bmatrix} 21.7 & -0.2 & -0.5 \\ -0.2 & 22.3 & -0.3 \\ -0.5 & -0.3 & 25.5 \end{bmatrix} \text{kg}\cdot\text{m}^2. \quad (85)$$

The leader spacecraft moves on a Molniya orbit, and its initial orbital elements are given in Table 1 [3].

Assuming that the leader spacecraft moves along an ideal orbit, its orbit is generated by offline calculation. At the

initial moment, the body-fixed frame of the leader spacecraft coincides with the orbital coordinate system, and its initial pose configuration and initial velocity are

$$\mathbf{g}_o = \begin{bmatrix} 0.8660 & -0.5 & 0 & 16490.0 \\ 0.2239 & 0.3878 & -0.8942 & 4262.8 \\ 0.4471 & 0.7744 & 0.4478 & 8512.6 \\ 0 & 0 & 0 & 1 \end{bmatrix}, \quad (86)$$

$$\xi_o = [3.7052 \ 3.6292 \ 0 \ 0 \ 0 \ 0.0011]^T.$$

The position vector is expressed in the ECI system, and its unit is km, and the velocity vector is expressed in the body-fixed coordinate system, and the units are rad/s and km/s.

The definition of the initial pose configuration and initial velocity parameters of the follower spacecraft relative to the leader spacecraft are shown in Table 2.

The desired pose configuration and desired velocity of the follower spacecraft relative to the leader spacecraft are shown in Table 3.

In other words, the control goal is to keep the attitude synchronization between the follower spacecraft and the leader spacecraft, hover under it, and the relative velocity of the two is zero.

The uncertain part of the mass and inertia matrix and the external disturbances are selected as follows:

$$\Delta\Gamma = \text{diag}(\sin(0.5t)\mathbf{I}_3, 0.1 \sin(0.5t)\mathbf{I}_3),$$

$$\Gamma_d = \begin{bmatrix} 0.05 \sin(0.5t)\text{N} \\ 0.05 \sin(0.5t)\text{N} \\ -0.05 \sin(0.5t)\text{N} \\ 0.005 \sin(0.15t)\text{N} \cdot \text{m} \\ 0.005 \sin(0.25t)\text{N} \cdot \text{m} \\ -0.005 \sin(0.2t)\text{N} \cdot \text{m} \end{bmatrix}. \quad (87)$$

During the simulation, the maximum output of the reaction flywheel and thruster are 1 N.m and 10 N, respectively. That is, the boundary of control force is $[-10, 10]\text{N}$, and the control torque is limited to $[-1, 1]\text{N} \cdot \text{m}$. The parameters of the controllers are chosen as in Table 4.

The specific fault types of each flywheel and each thruster are shown in Table 5.

Figures 4–7 show the output of AF-MFixed and its comparison with AF-Finite and AF-Fixed under the normal condition of the actuator; Figures 8–11 show the output with the actuator fault. The above output results verify the stability analysis of the proposed control scheme.

Figure 4 illustrates the pose configuration and the velocity tracking error of AF-MFixed without actuator fault. It can be seen that the attitude and angular velocity tracking errors quickly converge to the equilibrium state within 18 s, and the convergence accuracy is finally maintained within $1 \times 10^{-4}\text{deg}$ and $2 \times 10^{-5}\text{deg/s}$, respectively; the position and translational velocity tracking errors quickly converge to the equilibrium state within 60 s, and the convergence

TABLE 1: Initial orbital elements of the leader.

Orbital element	Value
Semimajor axis (km) a (km)	26628
Eccentricity e	0.7417
Inclination i (deg)	63.4
RAAN Ω (deg)	0
Argument of perigee ω (deg)	270
True anomaly f (deg)	120

TABLE 2: Initial state of the follower spacecraft relative to the leader spacecraft.

Initial relative parameters	Values
Initial relative position (m)	$[15 \ 15 \ 15]^T$
Initial relative linear velocity (m/s)	$[-0.051 \ -0.247 \ -0.075]^T$
Initial relative attitude (rad)	$2\pi/3$
Initial relative principal rotation axis	$[-2 \ -2 \ -3]^T$
Initial relative angular velocity (rad/s)	$[0.009 \ 5.98 \ -9.31]^T \times 10^{-4}$

accuracy is finally maintained within 8×10^{-5} m and 1×10^{-6} m/s, respectively.

Figure 5(a) shows the output torque of each flywheel and Figure 5(b) shows the output force of each thruster under normal conditions. It is evident that all the actuator outputs are bounded.

Figure 6 shows the comparison of the pose configuration and the velocity tracking error norms among AF-Finite, AF-Fixed, and AF-MFixed without actuator fault. It can be seen from Figures 6(a) and 6(b) that the convergence rates and convergence accuracy of the three methods are almost the same for attitude and angular velocity tracking errors. From Figures 6(c) and 6(d), as for position and translational velocity tracking errors, AF-MFixed and AF-Fixed are superior to AF-Finite in convergence rates, AF-Finite have the highest convergence accuracy of position tracking error, and the minimum overshoot of translational velocity tracking error, but it has the lowest convergence accuracy of translational velocity tracking error, and the control performance of AF-Fixed is between the other two. In summary, AF-MFixed has more obvious advantages in terms of rapidity than AF-Finite and accuracy of control performance than AF-Fixed, which also confirms the analysis and discussion of AF-MFixed in Remark 2.

Figure 7 shows the comparison of the integration of control force and torque of the three methods without actuator fault. The integral of the control output often represents the control energy. From Figure 7(a), we can know that AF-Finite has the largest energy consumption of control force (integration of control force) and AF-Fixed and AF-MFixed have the similar control force energy consumption. However, it can be seen from Figure 7(b) that there is no significant difference in the energy consumption of control torque (integration of control torque) among the three. Therefore, AF-MFixed also has great advantages in reducing control energy consumption.

Figure 8 illustrates the pose configuration and the velocity tracking error of AF-MFixed with actuator fault. It can

TABLE 3: Desired state of the follower spacecraft relative to the leader spacecraft.

Desired relative parameters	Values
Desired relative position (m)	$[5 \ 0 \ 0]^T$
Desired relative linear velocity (m/s)	$[0 \ 0 \ 0]^T$
Desired relative attitude (rad)	0
Desired relative angular velocity (rad/s)	$[0 \ 0 \ 0]^T$

TABLE 4: Control parameters for simulation.

Parameter name	Values
Sliding surface	$\alpha = 0.6, \alpha_1 = 1.2, \alpha_2 = 0.6$ $C_1 = \text{diag}(0.054, 0.054, 0.054, 0.18, 0.18, 0.18)$ $C_2 = \text{diag}(0.054, 0.054, 0.054, 0.18, 0.18, 0.18)$ $K_1 = \text{diag}(1200, 800, 800, 10, 10, 10)$
Controller parameters	$K_2 = \text{diag}(1200, 800, 800, 10, 10, 10)$ $\gamma = 0.001$

TABLE 5: Fault conditions of actuators.

Actuator	Fault expression
Flywheel 1	$u_1 = \begin{cases} u_{1c} & t < 25 \text{ s} \\ 0.65u_{1c} & t \geq 25 \text{ s} \end{cases}$
Flywheel 2	$u_2 = \begin{cases} u_{2c} & t < 25 \text{ s} \\ 0.5u_{2c} & t \geq 25 \text{ s} \end{cases}$
Flywheel 3	$u_3 = 0.8u_{3c}, t > 0 \text{ s}$
Flywheel 4	$u_4 = 0.6u_{4c}, t > 0 \text{ s}$
Thruster 1	$u_5 = \begin{cases} 0 \text{ N} & t < 15 \text{ s} \\ 0.4u_{5c} & t \geq 15 \text{ s} \end{cases}$
Thruster 2	$u_6 = 0.9u_{6c}, t > 0 \text{ s}$
Thruster 3	$u_7 = \begin{cases} 0 \text{ N} & t < 15 \text{ s} \\ 0.6u_{7c} & t \geq 15 \text{ s} \end{cases}$
Thruster 4	$u_8 = 0.75u_{8c}, t > 0 \text{ s}$
Thruster 5	$u_9 = \begin{cases} u_{9c} & t < 1 \text{ s} \\ 0.8u_{9c} & t \geq 15 \text{ s} \end{cases}$
Thruster 6	$u_{10} = 0.3u_{10c}, t > 0 \text{ s}$
Thruster 7	$u_{11} = \begin{cases} u_{11c} & t < 15 \text{ s} \\ 0.6u_{11c} & t \geq 15 \text{ s} \end{cases}$
Thruster 8	$u_{12} = 0.45u_{12c}, t > 0 \text{ s}$

be seen that the attitude and angular velocity tracking errors quickly converge to the equilibrium state within 20 s, and the convergence accuracy is finally maintained within 3×10^{-4} deg and 2×10^{-5} deg/s, respectively. The position tracking errors quickly converge to the equilibrium state within 60 s, and the convergence accuracy is finally maintained within 4×10^{-3} m and tends to decrease; the translational velocity tracking errors quickly converge to the equilibrium state within 75 s, and the convergence accuracy is finally maintained within 2×10^{-5} m/s.

Figure 9(a) shows the output torque of each flywheel, and Figure 9(b) shows the output force of each thruster under fault conditions. It is evident that all the actuator outputs are bounded, and the output curves well reflect the types of the fault. It is worth noting that the control torques and forces do not vanish completely when the control goal is

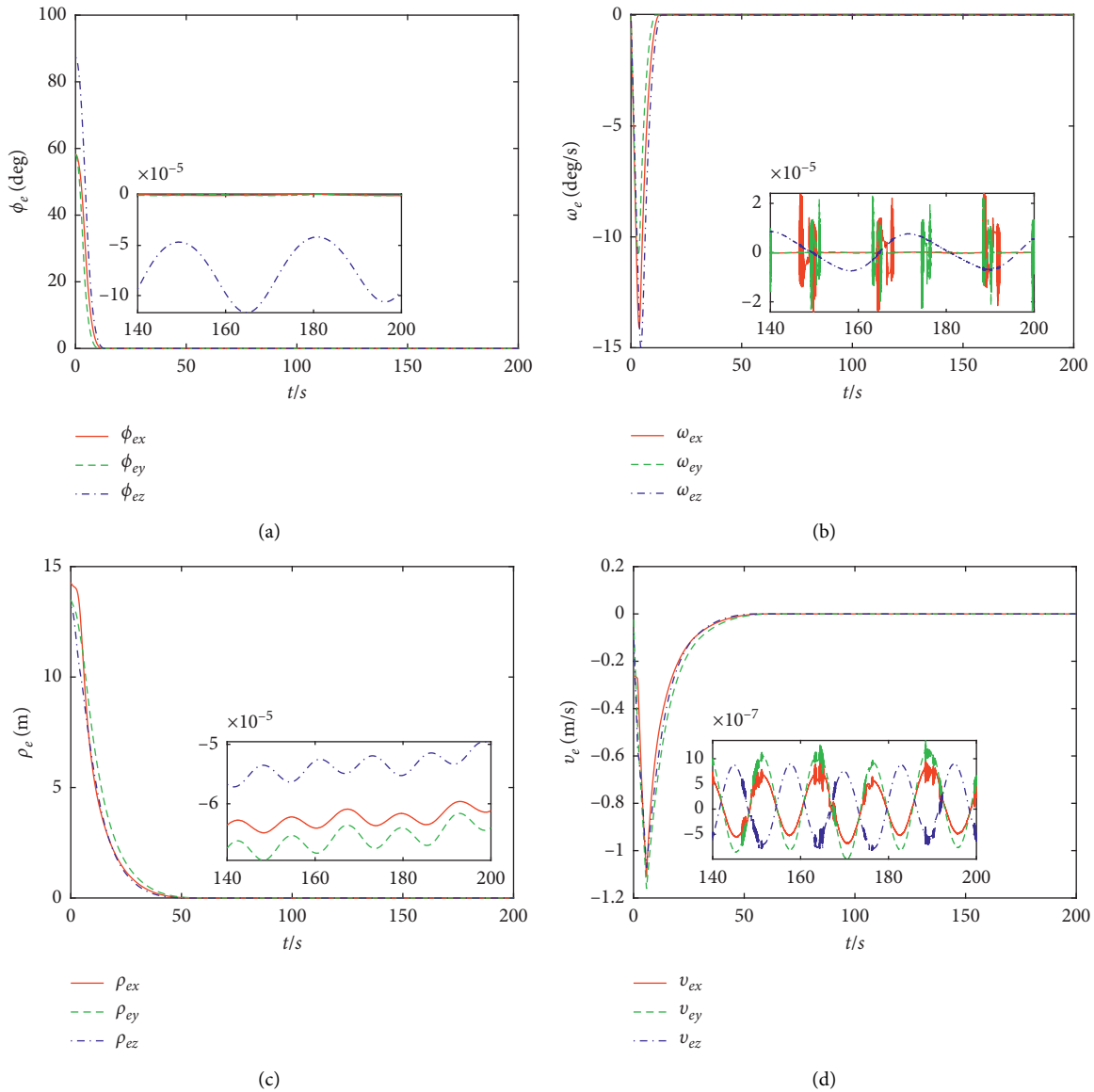


FIGURE 4: Tracking errors of AF-MFixed under normal condition.

achieved because they also need to compensate for the total disturbances and actuator faults to keep the relative pose configuration between the follower spacecraft and the leader spacecraft.

Figure 10 shows the comparison of the pose configuration and the velocity tracking errors norms among AF-Finite, AF-Fixed, and AF-MFixed with actuator fault. It can be seen from Figures 10(a) and 10(b) that the convergence rates of the three methods are almost the same for attitude and angular velocity tracking errors, but AF-MFixed has a significant advantage over AF-Fixed in terms of convergence accuracy for attitude tracking error. We can know from

Figures 10(a) and 10(c) that AF-Finite has the highest convergence accuracy for relative pose configuration tracking error. From Figures 10(c) and 10(d), as for position and translational velocity tracking errors, AF-M-Fixed and AF-Fixed are superior to AF-Finite in convergence rates, AF-Finite have the highest convergence accuracy of position and translational velocity tracking error and the minimum overshoot of translational velocity tracking error, the control performance of AF-Fixed is between the other two, and it can realize the translational velocity tracking error control with high accuracy and convergence rates, but AF-MFixed can converge more

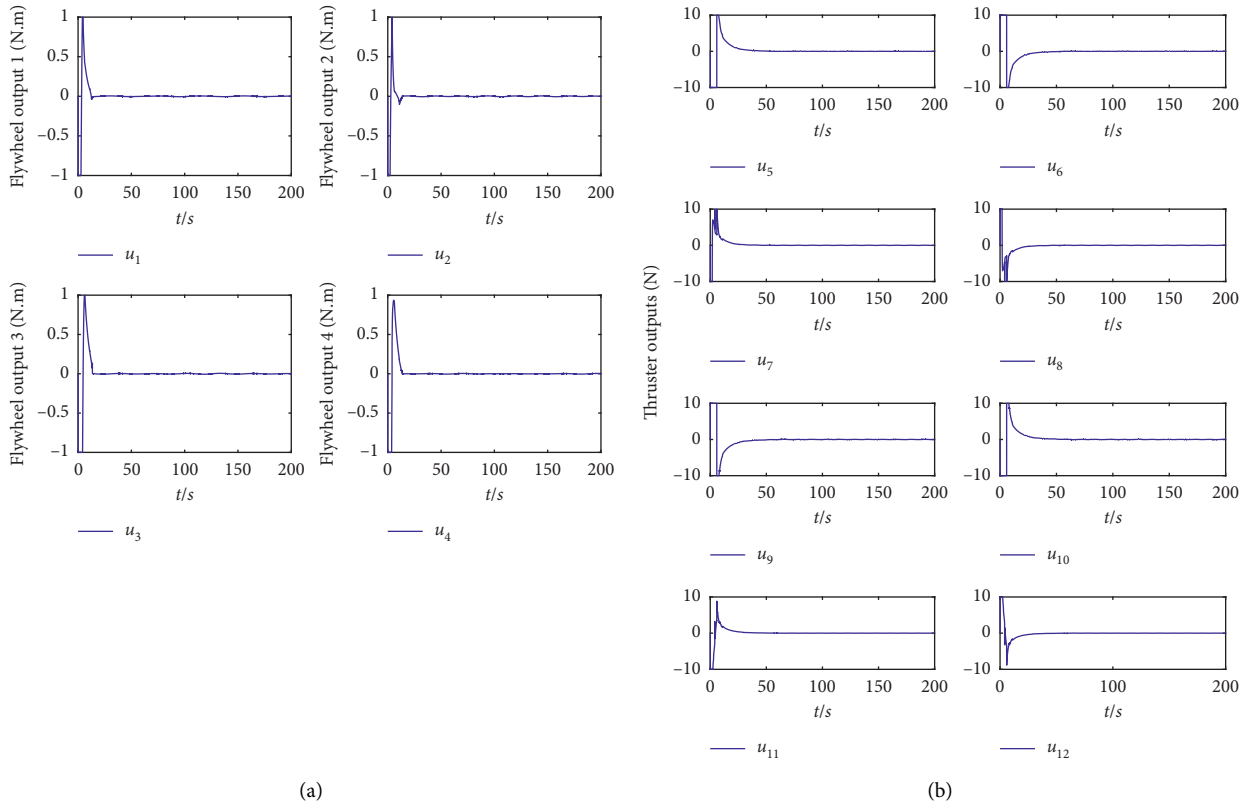


FIGURE 5: Tracking errors of AF-MFixed under normal condition.

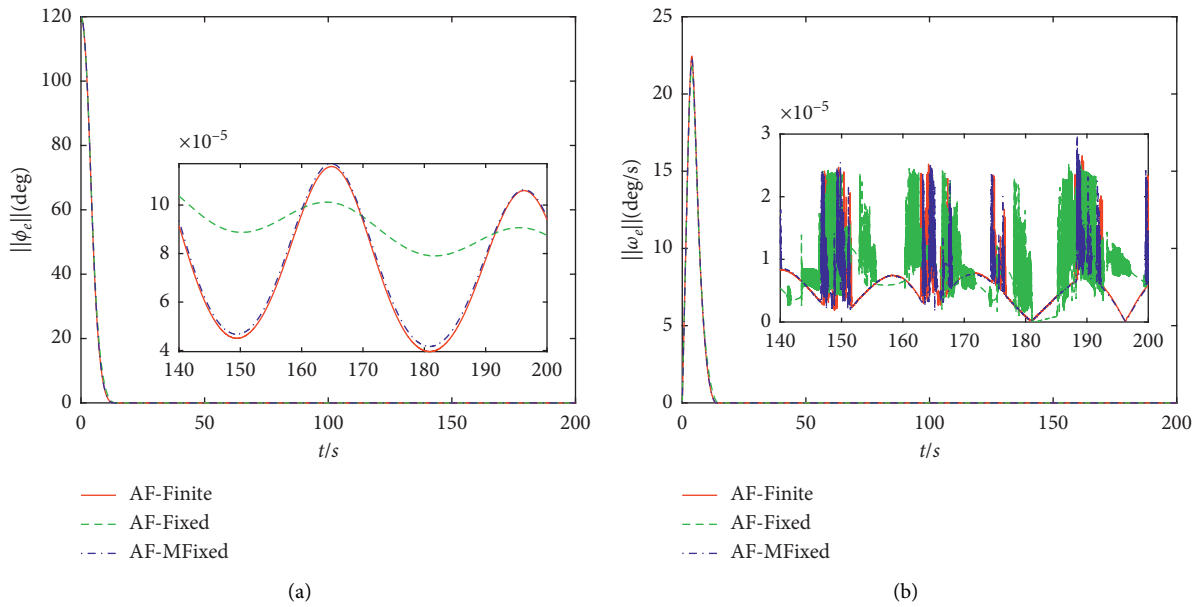


FIGURE 6: Continued.

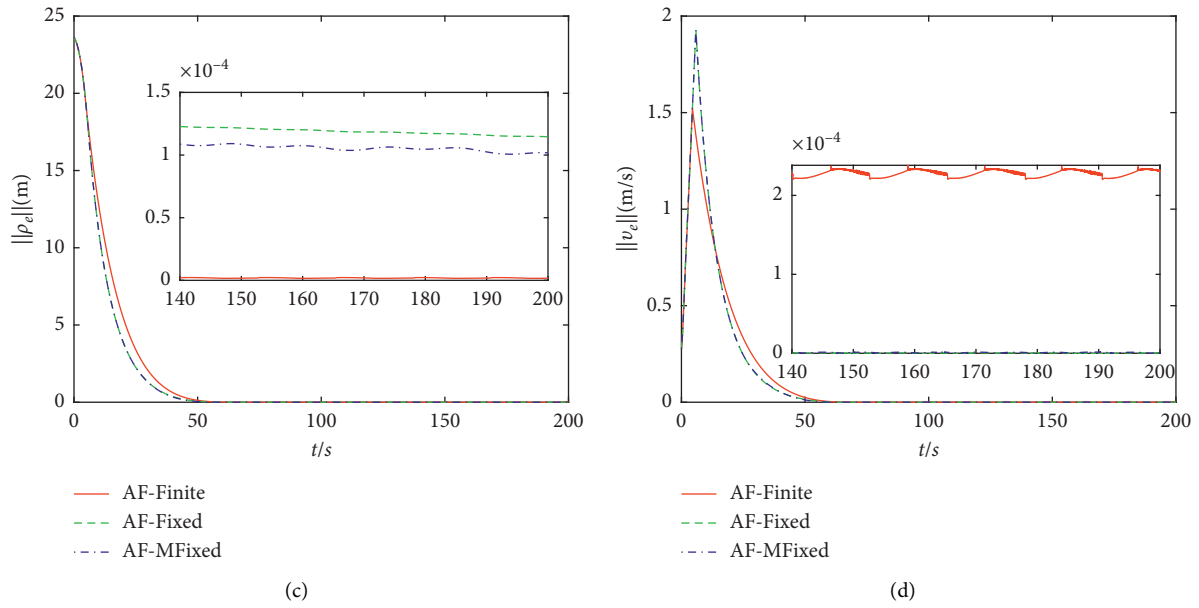


FIGURE 6: Comparison of the tracking error output norms of the three methods under normal condition.

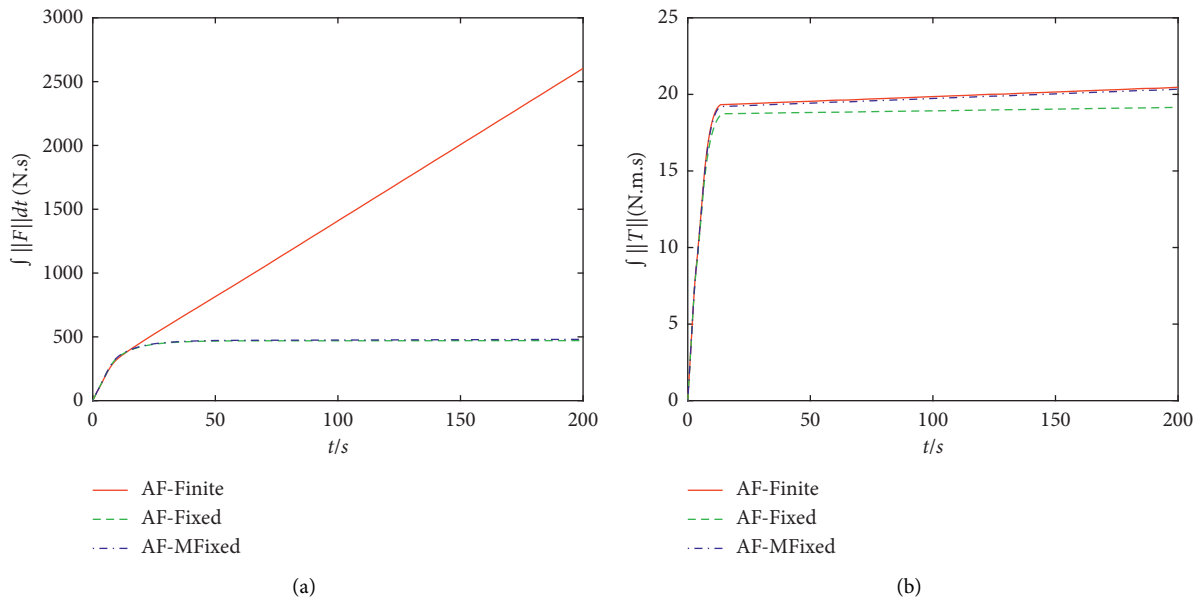


FIGURE 7: Comparison of the integration of control output of the three methods under normal condition.

accurately than AF-Fixed at the same convergence speed. In summary, AF-MFixed has more obvious advantages in terms of rapidity and accuracy of control performance, which also confirms the analysis and discussion of AF-MFixed in Remark 2.

Figure 11 shows the comparison of the integration of control force and torque of the three methods with actuator

fault. From Figure 11(a), we can know that AF-Finite has the lowest energy consumption of control force, and AF-MFixed is slightly higher than that of AF-Fixed in order to achieve fast convergence performance. However, it can be seen from Figure 11(b) that AF-Fixed has the lowest energy consumption of control torque, and AF-Finite is slightly higher than that of AF-Fixed, but the difference in the

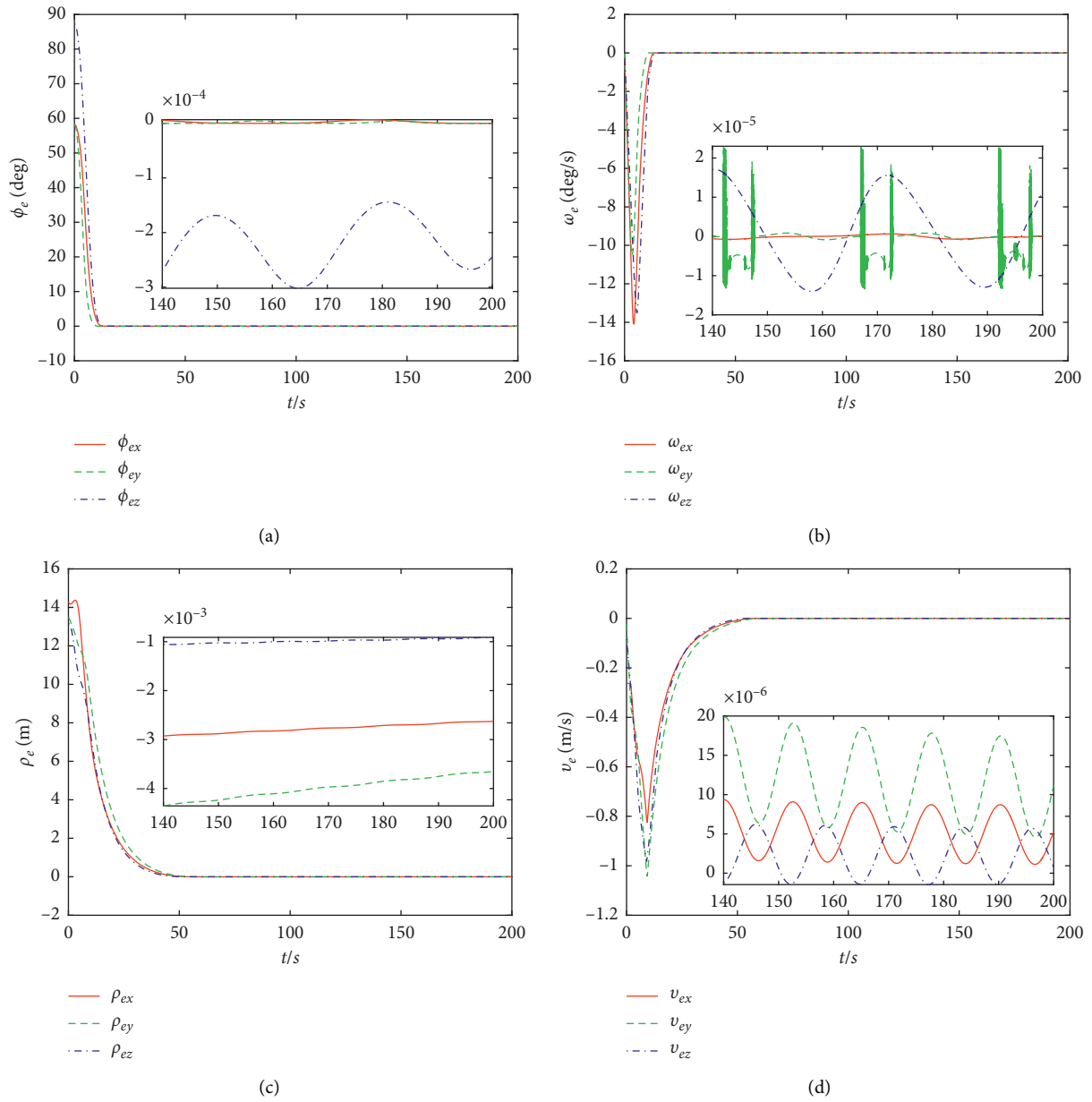


FIGURE 8: Tracking errors of AF-MFixed with actuator fault.

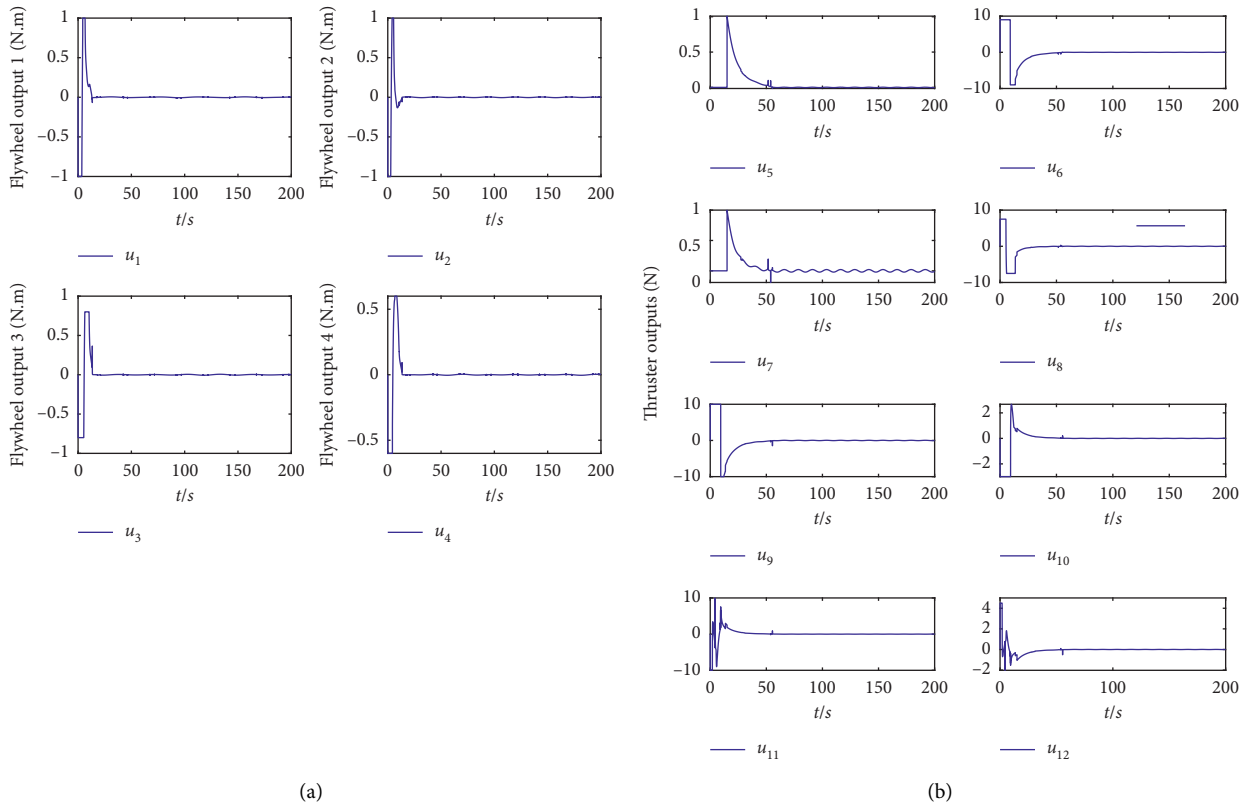


FIGURE 9: Output of actuators under fault condition.

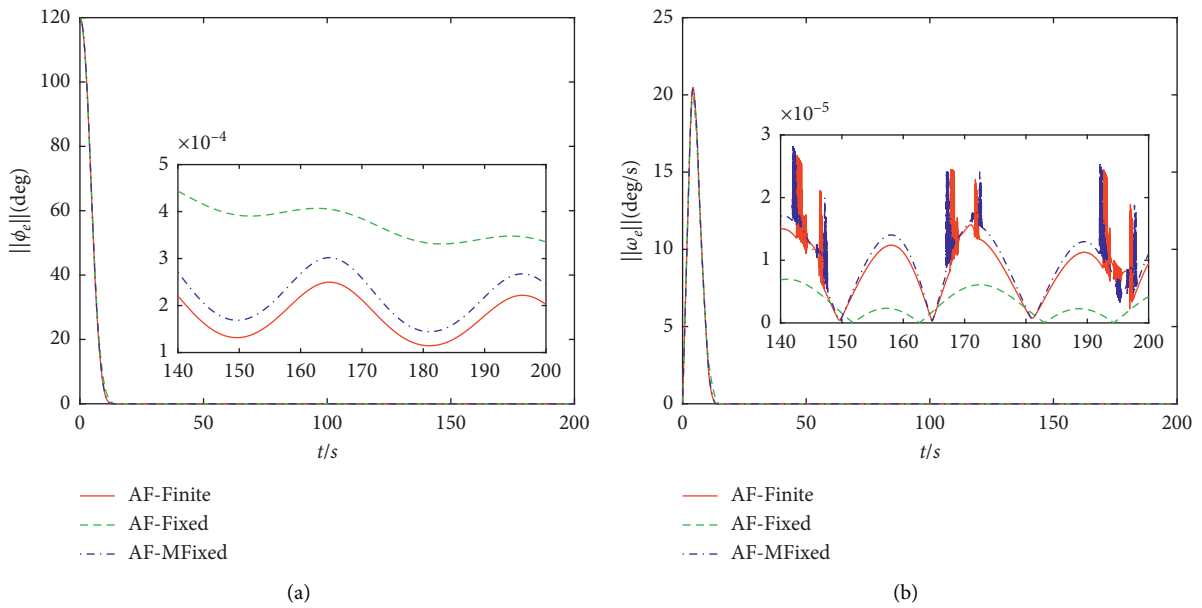


FIGURE 10: Continued.

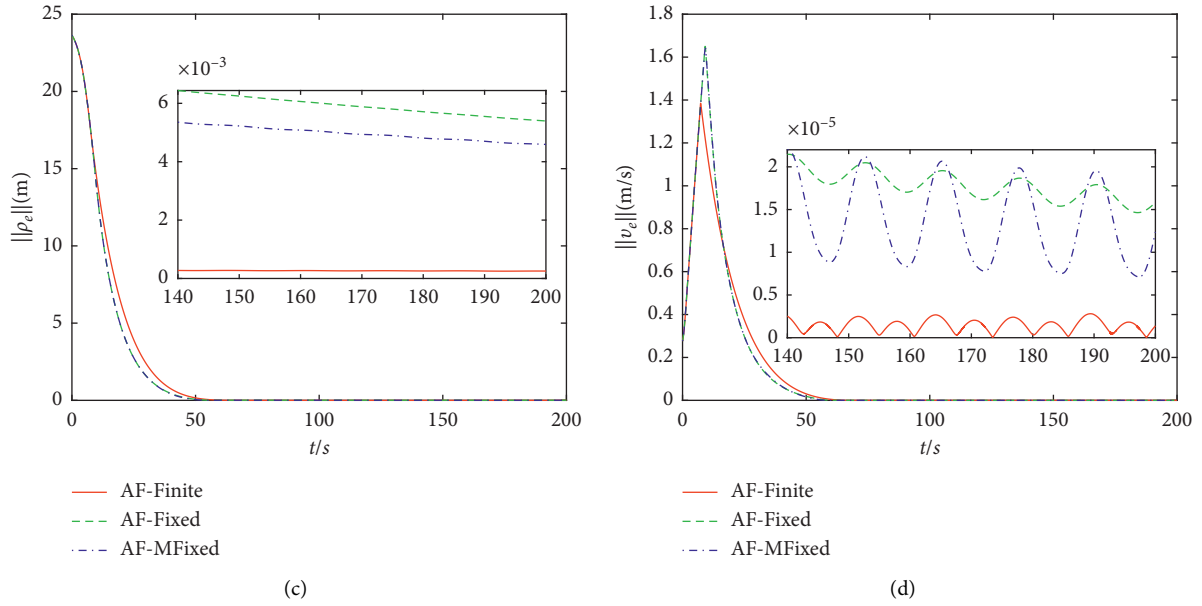


FIGURE 10: Comparison of the tracking error output norms of the three methods with actuator fault.

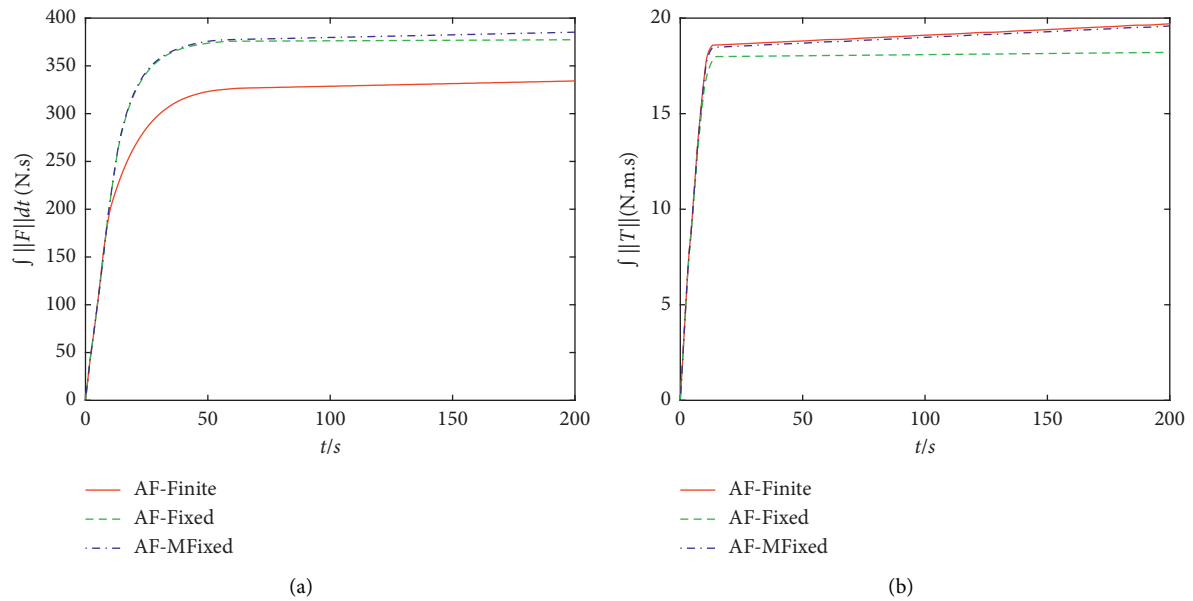


FIGURE 11: Comparison of the integration of control output of the three methods with actuator fault.

energy consumption of control torque is not obvious among the three compared with energy consumption of control force.

5. Conclusions

In this paper, adaptive fuzzy modified Fixed-time fault-tolerant control schemes on SE(3) for coupled spacecraft were proposed to solve the attitude and position tracking

problem with external disturbances, model uncertainties, and actuator faults simultaneously. From the comparative analysis of the three control strategies, we can see that AF-MFixed can achieve the control goals of fast convergence and higher tracking accuracy; the settling time of the closed-loop tracking system can be independent of the initial states. The integrated attitude and position modeling method based on Lie group SE(3) is simple and can be applied to solve the problem of 6-DOF in practical aerospace engineering. The

fuzzy adaptive control scheme can estimate the total disturbances and fault information with high accuracy. The parameter tuning of the proposed algorithm is simple, avoiding the tedious adjustment of too many parameters. Moreover, the algorithm is suitable for both actuator failure and normal condition, and the control performance under fault condition will be slightly lower than that under normal condition, which also shows that the robustness proposed in this paper has a strong advantage, and it has potential engineering application value. However, the practical problem is that the actuator fault information is difficult to obtain in real time. The establishment of a fault observer for fault diagnosis will be the work of the author in the future, and the estimated fault information will be applied to the design of fault-tolerant controllers. In addition, the next research content of this paper will consider the influence of sensor measurement noise and fault, and design a more robust fault-tolerant controller.

Data Availability

The data used to support the findings of this study are included in this paper.

Conflicts of Interest

The authors declare that there are no conflicts of interest regarding the publication of this paper.

Acknowledgments

This research was funded by the Shanghai Aerospace Science and Technology Innovation Foundation, Grant No. SAST2020-023.

References

- [1] M. S. De Queiroz, V. Kapila, and Q. Yan, "Adaptive nonlinear control of multiple spacecraft formation flying," *Journal of Guidance, Control, and Dynamics*, vol. 23, no. 3, pp. 385–390, 2000.
- [2] D. Lee, "Spacecraft coupled tracking maneuver using sliding mode control with input saturation," *Journal of Aerospace Engineering*, vol. 28, no. 5, Article ID 04014136, 2014.
- [3] K. Gong, Y. Y. Liao, and Y. Wang, "Adaptive fixed-time terminal sliding mode control on SE(3) for coupled spacecraft tracking maneuver," *International Journal of Aerospace Engineering*, vol. 2020, pp. 1–15, 2020.
- [4] Z. Chen, Q. Chen, X. He et al., "Adaptive finite-time command filtered fault-tolerant control for uncertain spacecraft with prescribed performance," *Complexity*, vol. 2018, 2018.
- [5] F. Song and S. Qin, "robust fault-tolerant control for satellite attitude stabilization based on active disturbance rejection approach with artificial bee colony algorithm," *Mathematical Problems in Engineering*, vol. 2014, no. 4, 17 pages, Article ID 512707, 2014.
- [6] J. Zhang, D. Ye, Z. Sun et al., "Extended state observer based robust adaptive control on SE(3) for coupled spacecraft tracking maneuver with actuator saturation and misalignment," *Acta Astronautica*, vol. 143, 2018.
- [7] H. Dong, Q. Hu, M. I. Friswell, and G. Ma, "Dual-quaternion-based fault-tolerant control for spacecraft tracking with finite-time convergence," *IEEE Transactions on Control Systems Technology*, vol. 25, no. 4, pp. 1231–1242, 2017.
- [8] H. Dong, Q. Hu, and G. Ma, "Dual-quaternion based fault-tolerant control for spacecraft formation flying with finite-time convergence," *ISA Transactions*, vol. 61, no. Mar., pp. 87–94, 2016.
- [9] D. Lee, A. K. Sanyal, and E. A. Butcher, "Asymptotic tracking control for spacecraft formation flying with decentralized collision avoidance," *Journal of Guidance, Control, and Dynamics*, vol. 38, no. 4, pp. 587–600, 2015.
- [10] D. Lee and G. Vukovich, "Almost global finite-time stabilization of spacecraft formation flying with decentralized collision avoidance," *International Journal of Control, Automation and Systems*, vol. 15, no. 3, pp. 1167–1180, 2017.
- [11] M. R. Binette, C. J. Damaren, and L. Pavel, "Nonlinear H ∞ attitude control using modified Rodrigues parameters," *Journal of Guidance, Control, and Dynamics*, vol. 37, no. 6, pp. 2017–2021, 2014.
- [12] Y. Huang and Y. Jia, "Robust adaptive fixed-time tracking control of 6-DOF spacecraft fly-around mission for noncooperative target," *International Journal of Robust and Nonlinear Control*, vol. 28, no. 6, pp. 2598–2618, 2018.
- [13] J. Zhang, D. Ye, J. D. Biggs, and Z. Sun, "Finite-time relative orbit-attitude tracking control for multi-spacecraft with collision avoidance and changing network topologies," *Advances in Space Research*, vol. 63, no. 3, pp. 1161–1175, 2019.
- [14] D. Lee, A. Sanyal, E. Butcher, and D. Scheeres, "Finite-time control for spacecraft body-fixed hovering over an asteroid," *IEEE Transactions on Aerospace and Electronic Systems*, vol. 51, no. 1, pp. 506–520, 2015.
- [15] A. Sanyal, L. Holguin, and S. P. Viswanathan, "Guidance and control for spacecraft autonomous chasing and close proximity maneuvers," *IFAC Proceedings Volumes*, vol. 45, no. 13, pp. 753–758, 2012.
- [16] F. Bullo and R. M. Murray, *Proportional Derivative (Pd) Control on the Euclidean Group*, vol. 2, pp. 1091–1097, European Control Conference CiteSeer, Zurich, Switzerland, 1995.
- [17] L. Jiang, Y. Wang, and S. Xu, "Integrated 6-DOF orbit-attitude dynamical modeling and control using geometric mechanics," *International Journal of Aero-Space Engineering*, vol. 2017, no. 1, 13 pages, Article ID 4034328, 2017.
- [18] J. Ackermann, "Parameter space design of robust control systems," *IEEE Transactions on Automatic Control*, vol. 25, no. 6, pp. 1058–1072, 1980.
- [19] D. Zhao, H. Yang, B. Jiang, and L. Wen, "Attitude stabilization of a flexible spacecraft under actuator complete failure," *Acta Astronautica*, vol. 123, pp. 129–136, 2016.
- [20] H. Qian, M. Y. Peng, and M. Cui, "Adaptive observer-based fault-tolerant control design for uncertain systems," *Mathematical Problems in Engineering*, vol. 2015, no. 3, 16 pages, Article ID 429361, 2015.
- [21] G. Q. Wu, S. N. Wu, and Z. G. Wu, "Robust finite-time control for spacecraft with coupled translation and attitude dynamics," *Mathematical Problems in Engineering*, vol. 2013, no. 4, 7 pages, Article ID 707485, 2013.
- [22] L. Zheng, Q. X. Dong, and X. M. YangZeng, "Robust adaptive sliding mode fault tolerant control for nonlinear system with actuator fault and external disturbance," *Mathematical Problems in Engineering*, vol. 2019, Article ID 6349510, 13 pages, 2019.
- [23] K. Zhou and Y. Xia, "Adaptive attitude tracking control for rigid spacecraft with finite-time convergence," *Automatica*, vol. 49, no. 12, pp. 3591–3599, 2013.

- [24] T. Wang, J. Qiu, S. Yin, H. Gao, J. Fan, and T. Chai, "Performance-based adaptive fuzzy tracking control for networked industrial processes," *IEEE Transactions on Cybernetics*, vol. 46, no. 8, pp. 1760–1770, 2016.
- [25] T. Wang, H. Gao, and J. Qiu, "A combined adaptive neural network and nonlinear model predictive control for multirate networked industrial process control," *IEEE Transactions on Neural Networks and Learning Systems*, vol. 27, no. 2, pp. 416–425, 2015.
- [26] L. Li, S. X. Ding, J. Qiu, Y. Yang, and Y. Zhang, "Weighted fuzzy observer-based fault detection approach for discrete-time nonlinear systems via piecewise-fuzzy Lyapunov functions," *IEEE Transactions on Fuzzy Systems*, vol. 24, no. 6, pp. 1320–1333, 2016.
- [27] L. Li, S. X. Ding, J. Qiu, and Y. Yang, "Real-time fault detection approach for nonlinear systems and its asynchronous T-S fuzzy observer-based implementation," *IEEE Transactions on Cybernetics*, vol. 47, no. 2, pp. 283–294, 2017.
- [28] Y. Wei, J. Qiu, and H.-K. Lam, "A novel approach to reliable output feedback control of fuzzy-affine systems with time delays and sensor faults," *IEEE Transactions on Fuzzy Systems*, vol. 25, no. 6, p. 1808, 2017.
- [29] Y. Wei, J. Qiu, H. K. Lam, and L. Wu, "Approaches to T-S fuzzy-affine-model-based reliable output feedback control for nonlinear ITO stochastic systems," *IEEE Transactions on Fuzzy Systems*, vol. 25, 2017.
- [30] A.-M. Zou and K. D. Kumar, "Adaptive fuzzy fault-tolerant attitude control of spacecraft," *Control Engineering Practice*, vol. 19, no. 1, pp. 10–21, 2011.
- [31] B. Huo, Y. Xia, K. Lu, and M. Fu, "Adaptive fuzzy finite-time fault-tolerant attitude control of rigid spacecraft," *Journal of the Franklin Institute*, vol. 352, no. 10, pp. 4225–4246, 2015.
- [32] J. Zhang, M. D. Ye, and Z. Sun, "Adaptive fuzzy finite-time control for spacecraft formation with communication delays and changing topologies," *Journal of the Franklin Institute*, vol. 354, no. 11, pp. 4377–4403, 2017.
- [33] S. T. Venkataraman and S. Gulati, "Control of nonlinear systems using terminal sliding modes," *Journal of Dynamic Systems, Measurement, and Control*, vol. 115, no. 3, pp. 554–560, 1993.
- [34] X. Yu and M. Zhihong, "Fast terminal sliding-mode control design for nonlinear dynamical systems," *IEEE Transactions on Circuits and Systems—I: Fundamental Theory and Applications*, vol. 49, no. 2, pp. 261–264, 2002.
- [35] L. Yang and J. Yang, "Nonsingular fast terminal sliding-mode control for nonlinear dynamical systems," *International Journal of Robust and Nonlinear Control*, vol. 21, no. 16, pp. 1865–1879, 2011.
- [36] X. N. Shi, Z. G. Zhou, and D. Zhou, "Adaptive fault-tolerant attitude tracking control of rigid spacecraft on Lie group with fixed time convergence," *Asian Journal of Control*, vol. 22, no. 1, pp. 423–435, 2020.
- [37] X.-N. Shi, Y.-A. Zhang, D. Zhou, and Z.-G. Zhou, "Global fixed-time attitude tracking control for the rigid spacecraft with actuator saturation and faults," *Acta Astronautica*, vol. 155, pp. 325–333, 2019.
- [38] J. W. Gao, Z. Fu, and S. Zhang, "Adaptive fixed-time attitude tracking control for rigid spacecraft with actuator faults," *IEEE Transactions on Industrial Electronics*, vol. 66, 2019.
- [39] S. Mobayen, J. Ma, G. Pujol-Vázquez, L. Acho, and Q. Zhu, "Adaptive finite-time stabilization of chaotic flow with a single unstable node using a nonlinear function-based global sliding mode," *Iranian Journal of Science and Technology, Transactions of Electrical Engineering*, vol. 43, no. S1, pp. 339–347, 2019.
- [40] S. Mobayen and G. Pujol-Vázquez, "A robust LMI approach on nonlinear feedback stabilization of continuous state-delay systems with lipschitzian nonlinearities: experimental validation," *Iranian Journal of Science and Technology, Transactions of Mechanical Engineering*, vol. 43, no. 3, pp. 549–558, 2019.
- [41] M. Jafari and S. Mobayen, "Second-order sliding set design for a class of uncertain nonlinear systems with disturbances: an LMI approach," *Mathematics and Computers in Simulation*, vol. 156, pp. 110–125, 2019.